

Article

# Extremal Solutions for Surface Energy Minimization: Bicubically Blended Coons Patches

Daud Ahmad <sup>1,\*</sup> , Kiran Naz <sup>1</sup>, Mariyam Ehsan Buttar <sup>1</sup>, Pompei C. Darab <sup>2</sup>  and Mohammed Sallah <sup>3,4</sup> 

<sup>1</sup> Department of Mathematics, University of the Punjab, Lahore 54590, Pakistan; kirantariq1993@gmail.com (K.N.); mariyambuttar786@gmail.com (M.E.B.)

<sup>2</sup> Department of Electric Power Systems and Management, Faculty of Electrical Engineering, Technical University of Cluj-Napoca, 400001 Cluj-Napoca, Romania; cosmin.darab@eps.utcluj.ro

<sup>3</sup> Applied Mathematical Physics Research Group, Physics Department, Faculty of Science, Mansoura University, Mansoura 35516, Egypt; msallahd@mans.edu.eg

<sup>4</sup> Higher Institute of Engineering and Technology, New Damietta 34517, Egypt

\* Correspondence: daud.math@pu.edu.pk

**Abstract:** A Coons patch is characterized by a finite set of boundary curves, which are dependent on the choice of blending functions. For a bicubically blended Coons patch (BBCP), the Hermite cubic polynomials (interpolants) are used as blending functions. A BBCP comprises information about its four corner points, including the curvature represented by eight tangent vectors, as well as the twisting behavior determined by the four twist vectors at these corner points. The interior shape of the BBCP depends not only on the tangent vectors at the corner points but on the twist vectors as well. The alteration in the twist vectors at the corner points can change the interior shape of the BBCP even for the same arrangement of tangent vectors at these corner points. In this study, we aim to determine the optimal twist vectors that would make the surface an extremal of the minimal energy functional. To achieve this, we obtain the constraints on the optimal twist vectors (MPDs) of the BBCP for the specified corner points by computing the extremal of the Dirichlet and quasi-harmonic functionals over the entire surface with respect to the twist vectors. These twist vectors can then be used to construct various quasi-minimal and quasi-harmonic BBCPs by varying corner points and tangent vectors. The optimization techniques involve minimizing a functional subject to certain constraints. The methods used to optimize twist vectors of BBCPs can have potential applications in various fields. They can be applied to fuzzy optimal control problems, allowing us to find the solution of complex and uncertain systems with fuzzy constraints. They provide us an opportunity to incorporate symmetry considerations for the partial differential equations associated with minimal surface equations, an outcome of zero-mean curvature for such surfaces. By exploring and utilizing the underlying symmetries, the optimization strategies can be further enhanced in terms of robustness and adaptability.

**Keywords:** optimal surfaces; symmetry considerations for optimal surfaces; optimal twist vectors; energy functionals; fuzzy differential equations; partial differential equations; computational geometry; bicubically blended Coons patches

**PACS:** JMSC2020:35B06; 49Q05; 53A10; 68U05



**Citation:** Ahmad, D.; Naz, K.; Buttar, M.E.; Darab, P.C.; Sallah, M. Extremal Solutions for Surface Energy Minimization: Bicubically Blended Coons Patches. *Symmetry* **2023**, *15*, 1237. <https://doi.org/10.3390/sym15061237>

Academic Editor: Ghulam Mustafa and Emmanuel Kengne

Received: 29 April 2023

Revised: 4 June 2023

Accepted: 5 June 2023

Published: 9 June 2023



**Copyright:** © 2023 by the authors. Licensee MDPI, Basel, Switzerland. This article is an open access article distributed under the terms and conditions of the Creative Commons Attribution (CC BY) license (<https://creativecommons.org/licenses/by/4.0/>).

## 1. Introduction

Optimization theory encompasses a wide range of disciplines, each with its unique focus and application in mathematics. In the field of calculus of variations, one can explore optimal solutions for functionals. Control theory, on the other hand, is concerned with optimizing system behavior. Convex optimization theory deals specifically with optimization problems involving convex constraints. Decision theory aims to make optimal decisions under uncertainty. Linear programming focuses on optimizing linear objective functions

subject to linear constraints. Network analysis, among other disciplines, is used to optimize the performance of networks. These diverse areas of study share a common objective: optimizing an objective function while satisfying a given constraint, often expressed in terms of an integral. It commonly involves working with functionals, such as integrals, over various domains and functions. In the realm of optimization theory, the overarching goal is twofold. First, it seeks to establish conditions within a domain (denoted by  $D$ ) that guarantee a solution to the optimization problem. Second, its objective is to analyze the optimal values, providing valuable insights into the function's behavior across the specified domain. The extreme values of objective function, known as optimal values, hold significant importance in numerous applications. One particularly active research area within optimization theory is the variational improvement in the objective functions. In the field of optimization theory, continuous exploration and development of techniques aim to enhance the performance and efficiency of objective functions, contributing to the overall advancement of optimization theory as a whole [1,2]. One example would be determining the shortest curve connecting two points, whose solution may be a straight line in the case of no constraints; however, constraints can cause multiple solutions to exist, known as geodesics. One instance is Hamilton's principle of least action. This principle is related to finding the time integral of the Lagrangian,  $\int_{t_1}^{t_2} L(t, q_s(t), \dot{q}_s(t)) dt$ , which is called the action integral. It is customary to write  $\delta \int_{t_1}^{t_2} L(t, q_s(t), \dot{q}_s(t)) dt = 0$  as the extremal of the action integral. The vanishing condition leads to the well-known Lagrange's equation of motion, a partial differential equation that describes the path of the particle. In Lagrange's equation, the Lagrangian  $L$  represents the difference between the system's kinetic and potential energy, while  $q_s(t)$  denotes the generalized coordinates necessary to describe the configuration space with the minimum number of coordinates. Hamilton's principle and Lagrange's equation hold significant importance in understanding the dynamics of physical systems in diverse fields of study. The famous action principle incorporates symmetries in its formulation. It has applications in the field of gravitation and electromagnetism, providing the equations of motion in these fields. Notably, the renowned Einstein field equations, which describe the behavior of gravity, can be obtained through the process of extremizing the Einstein–Hilbert action, which encompasses the symmetries of space-time [3]. For a detailed exposition on the connection between the action principle and Lagrangian formalism, and the derivation of the Einstein field equations, interested readers can refer to Section 21.2 of ref. [4].

In recent years, the exploration of symmetry in the analysis of geometric shapes and surfaces has gained significant attention. Symmetry can play a vital role in modeling the surfaces and for the better understanding of various related aspects or properties of shape perception. For instance, Jayadevan et al. [5] investigated the perception of symmetric and near-symmetric shapes by incorporating priors such as symmetry, compactness, and minimal surface and they have demonstrated the importance of symmetry-based metrics in accurately representing and analyzing the shapes. Similarly, Grundland and Hariton [6] extended the classical minimal surface equation to a supersymmetric form and examined the Lie superalgebra of symmetries associated with this extension and establish the rich interplay between symmetry and minimal surface theory. These works highlight the significance of symmetry as a fundamental principle in the analysis of geometric shapes and surfaces. Additionally, the symmetry groups of differential equations, as described in works such as [7–11], allow us to study the Lie group of symmetries associated with minimal surfaces. Bila [9] demonstrated that a minimal surface in Monge's form possesses a Lie group of symmetries generated by seven vector fields. Additionally, the works [12,13] provide valuable insights into the calculation of homotheties for various metric formulations, which could potentially be applied to analyze the metric for the BCP in this study.

The crucial role of symmetry in modeling and understanding various aspects of shape perception has been recognized in the field of variational methods. One notable problem related to variational methods is the *Plateau problem* [14,15], which entails seeking a surface with the smallest possible area among all surfaces bounded by a prescribed

boundary [16]. Minimal surfaces have a wide range of applications in surface design. They are also extensively used in other areas including materials science, civil engineering, and ship manufacturing, among other fields. The study of minimal surfaces [14,15], dating back to Lagrange (1762), involves the application of the Euler–Lagrange (EL) equation to find the surface  $z = z(u, v)$  with the minimal area among surfaces spanned by a given curve, utilizing a variational approach. However, he only found the plane as the solution. In 1776, Meusnier made a significant discovery regarding minimal surfaces. He found that the catenoid  $\mathbf{x}(u, v) = (c \cos u \cosh(v/c), c \sin u \cosh(v/c), v)$  and the helicoid  $\mathbf{x}(u, v) = (\rho \cos(\alpha\theta), \rho \sin(\alpha\theta), \theta)$  satisfy a fundamental equation closely tied to the mean curvature. This equation, which can be derived from the Euler–Lagrange equation, reveals that minimal surfaces exhibit zero mean curvature throughout. For surfaces given in the form of  $z = z(u, v)$ , the condition of vanishing mean curvature corresponds to the second-order partial differential equation:  $(1 + z_v^2)z_{uu} - 2z_u z_v z_{uv} + (1 + z_u^2)z_{vv} = 0$ . Solving this equation for the general solution  $z = z(u, v)$  poses challenges in the field. Mathematicians have made significant contributions to the study of minimal surfaces, exploring various scenarios that range from closed contours to boundaries composed of a finite number of curves. This includes the representation formulas found by Gaspard Monge and Legendre (1795), the Heinrich Scherk surfaces (1830), the work of Jesse Douglas [17], who minimized the Douglas functional (1931), Tibor Radó (1933) energy integral, and Shane’s (1933) saddle surface parameterization for minimal surfaces. Other significant contributions include the Plateau problem, Dirichlet’s principle, and higher-dimensional Plateau problems. Osserman and Nitsche [15,18] have provided a comprehensive survey of the characteristics of minimal surfaces. Numerical techniques, such as iterative methods and energy functionals, can also be employed to obtain quasi-minimal surfaces. These surfaces can be obtained numerically through iterative techniques, utilizing an ansatz for a slightly perturbed surface or by seeking the extremum of specific energy functionals. This approach avoids the need to directly solve a partial differential equation arising from the requirement of zero mean curvature for the surface [19–25].

Another interrelated problem involves the search for minimal surfaces, which are surfaces with the mean curvature equal to zero, among surfaces defined by prescribed boundary curves finite in number. These minimal surfaces have applications in various fields, not only in surface design but also in materials science and engineering disciplines like civil engineering and ship manufacturing [26–28]. To obtain a minimal surface using a variational technique for a surface defined by prescribed boundary curves, it is necessary to consider slightly perturbed surfaces that closely approximate the desired surface in terms of differential geometric properties. This approach has been explored in a previous study [19], focusing on a specific case of a Coons patch (Steven Anson Coons 1967). The Coons patch is constructed by spanning four distinct boundary curves and serves as a parameterization for interpolating the four boundary curves, connecting them at the four corner points. The behavior of the twist vectors at the corners plays a significant role in the construction of the Coons patch. The Coons patch is used to model a variety of physical problems and it has diverse applications in computer graphics and the related fields *CAGD*, *CAD*, *CAM*. Farouki et al. [29] present a method for constructing a  $C^2$  surface patch, utilizing bicubically blended Coons interpolation, in which the four specified boundary curves serve as geodesics of the surface. To achieve this, the authors establish global and local consistency constraints involving the variation of principal normals along the curves and the relationship between curvatures, torsions, and angles at the patch corners. Liu et al. [30] proposed the *SQ*-Coons surface, a parameterized surface in computer-aided design (CAD) that allows control over shape details through Bézier shape parameters. This surface is utilized in car design, specifically for optimizing aerodynamic performance by adjusting the control points and shape parameters to minimize the drag coefficient using computational fluid dynamics (CFD) analysis. A smoother surface can be achieved by utilizing bicubically blended interpolants, such as Hermite cubic polynomials, instead of bilinearly blending interpolants. Unlike a bilinearly blended Coons patch that relies on only four corner points

to connect the interpolating curves, a BBCP incorporates additional information in the form of tangent vectors and twist vectors computed for the corner points. This increased data allows for greater flexibility and control over the resulting surface. A specific instance of a BBCP is the Ferguson surface, which arises when the twist vectors are set to zero.

Various functionals [31–34] play an important role in studying different types of optimal surfaces. These functionals encompass a range of approaches, including the Dirichlet functional, which generates quasi-minimal surfaces. Additionally, the extended Dirichlet functional incorporates a parameter in its construction to obtain quasi-minimal surfaces. Both the quasi-harmonic functional and its extended version are employed to analyze quasi-harmonic surfaces. Moreover, the Willmore energy integral [35] serves as another important functional for analyzing Willmore surfaces. By utilizing these diverse functionals, one can explore and optimize various characteristics of surfaces within their respective domains. Furthermore, Xiaowei Li and colleagues [36] introduced an innovative algorithm for constructing Bézier surfaces with minimal diagonal energy. Their approach involved deriving necessary and sufficient conditions for the determination of interior control points. These conditions were established based on the linear relationship between the control points of diagonal curves and the resulting constructed surface. For an application of minimal surfaces, for instance, Bates et al. [37] find the mean curvature extremal of the molecular hypersurface function for the minimal molecular surface (MMS) for surface modeling of biomolecules to study the protein, membranes, DNA, and RNAs. These techniques are widely used as well for surface topography in grinding [38] using an algorithm [20]. Optimization techniques have been widely used in various applications, including microgrid operation planning and reducing occupant injury in vehicle crashes [39–41]. In the field of optimization, various techniques have been developed for solving problems involving optimality characteristics. Herty and Klar [42] proposed a modeling approach based on the numerical solution of conservation laws. In the context of process optimization, d'Apice et al. [43] proposed a mathematical model that integrates a control strategy to improve the performance of a process. Pinnau and Siedow [44] discussed an optimization problem that arises in the context of phase transitions, where the goal is to minimize the energy of the system. Marheineke et al. [45] presented a method for computing the gradient of the objective function in optimization problems, which is essential for many optimization algorithms. Marheineke and Pinnau [46] discussed a numerical method for solving an optimal control problem, where the objective is to find the optimal shape of a material. Drago et al. [47] proposed a numerical scheme for solving an optimization problem that arises in the design of semiconductor devices. These approaches illustrate the diversity of optimization techniques and their applications in various fields.

We have considered the use of the Dirichlet functional to analyze quasi-minimal surfaces and the quasi-harmonic functional to study harmonic surfaces. These functionals play a crucial role in identifying the extremals of the respective surfaces. It is worth noting the correlation between the concept of minimal surfaces (usually known as the 'Plateau problem') and the application of the Dirichlet functional. Similarly, the study of harmonic surfaces is associated with the utilization of the quasi-harmonic functional. In the context of the bicubically blended Coons patch, there are other ways, such as using Forrest's method to obtain the first twist vectors, bilinear surface formula, or Adini's method and then utilizing one of these techniques to construct the BBCP. These methods are elaborated upon in the subsequent section for reference. In our previous work [48], we have explained the method of finding the twist vectors for the BBCP in Section 5; specifically, Adini's method is given in Equations (50) and (51) for the twist vectors, utilizing Equation (49) for the tangent vectors. The respective twist vectors are given in Equation (52) of the same reference [48]. For a more comprehensive understanding of the twist vectors, we recommend referring to section (16.3) of ref. [49] and Sections (3.3.4) and (3.3.5) of ref. [50]. In our approach, however, we take a different route. Instead of explicitly computing the twist vectors using the aforementioned techniques, we consider the bicubically blended Coons patch with unspecified twist vectors computed at the four known corner points. By

treating this problem as an extremization of the Dirichlet functional and/or quasi-harmonic functional, our objective is to determine the optimal conditions for the twist vectors by solving the gradient vanishing condition with respect to these functionals. The condition of the gradient vanishing for functionals, such as the Dirichlet functional and the quasi-harmonic functional, imposes four linear constraints on the twist vectors. These constraints can be utilized to generate a near-minimal surface as the extremal of the Dirichlet functional and a quasi-harmonic Coons patch as the extremal of the quasi-harmonic functional. By solving these constraints and optimizing the twist vectors through integrals, the optimal twist vectors can be obtained. In the case where the mixed partial derivatives (MPDs) are set to zero within a surface patch, the resulting surface is known as a Ferguson surface. In Ferguson surfaces, the shape of the surface becomes flattened, while a surface with non-zero twist vectors at the four corners of the patch exhibits a rounded shape. The methods used to optimize twist vectors for BBCPs can also have applications in fuzzy optimal control problems and fuzzy differential equations. In the context of fuzzy calculus of variations, the fuzzy Euler–Lagrange equations characterize the extremal solutions of fuzzy variational problems. Therefore, by finding the extremal solutions of the Dirichlet and quasi-harmonic functionals for BBCPs, we can obtain the optimal twist vectors. This is similar to solving fuzzy control problems by finding the extremal solutions of fuzzy Euler–Lagrange equations. Some examples of previous works in this area include the fuzzy optimal control problem formulation by Filev and Angelov [51], the fuzzy Euler–Lagrange conditions derived by Farhadinia [52], and the study of fuzzy variational problems for the granular Euler–Lagrange equation by Mustafa et al. [53]. In the context of fuzzy differential equations, the Euler–Lagrange equations can be extended to fuzzy variational problems by using fuzzy derivative and integral operators. Therefore, the discussion of optimal surfaces and Euler–Lagrange equations in the context of variational calculus is related to fuzzy differential equations and fuzzy control problems through the concept of extremal solutions.

Various methods have been developed to tackle optimization problems under uncertainty in the field of fuzzy optimization. Puri and Ralescu [54] generalized the Rådström embedding theorem to define the concept of the differential of a fuzzy function. Sahinidis [55] provided an overview of various methods and techniques to tackle optimization problems under uncertainty. These include stochastic programming, robust optimization under uncertainty, fuzzy programming, and stochastic dynamic programming. Sahinidis discussed the advantages, shortcomings, and potential future developments of these methods in the field of optimization under uncertainty. In the context of fuzzy optimal control problems, Agarwal and Dumitru [56] presented a direct numerical technique for Fractional Optimal Control Problems (FOCPs) using Riemann–Liouville Fractional Derivatives (RLFDs) and the Grunwald–Letnikov definition, leading to a set of algebraic equations that can be solved using numerical techniques. Meanwhile, Agrawal [57] introduced an extension of the calculus of variations to include Caputo Fractional Derivatives (CFDs) and showed that fractional boundary conditions may be required even when Fractional Variational Problems (FVPs) are formulated in terms of CFDs only. In addition, there have been recent developments in the field of fuzzy and possibilistic optimization algorithms. Untiedt [58] investigated the effectiveness of various algorithms through their application to a well-known large-scale problem, the radiation therapy planning problem. The hybrid algorithms combine the strengths of fuzzy logic and optimization techniques, while incorporating computational models of the adaptive neuro-fuzzy inference system (ANFIS) that merge the adaptive capabilities of neural networks with the linguistic interpretability of fuzzy logic. In their study, Nguyen et al. [59] presented a bi-algorithm approach, utilizing a hybrid algorithm that combines fuzzy logic and ANFIS, for the design of a compliant gripper mechanism with multi-objective optimization. Their approach demonstrated enhanced effectiveness compared to conventional methods, surpassing traditional ideas such as material or shape modifications. Meanwhile, Huynh et al. [60] developed a method to optimize the magnification ratio of a flexible hinge displacement amplifier

mechanism through mathematical modeling and simulation, demonstrating the significant impact of design variables on the magnification ratio. Batool et al. [61] proposed efficient aggregation operators based on single-valued neutrosophic hesitant fuzzy sets for optimization and computational intelligence, which were demonstrated to be effective in a practical application for wireless charging station selection. Akram et al. [62] proposed novel methods, such as the Fermatean fuzzy DEA (FFDEA) method for solving the Fermatean fuzzy multi-objective transportation problem (MOTP), a new method for solving interval-valued Fermatean fuzzy fractional transportation problems (IVFFFTP) using triangular interval-valued Fermatean fuzzy numbers [63], and a compromise approach for solving the multi-objective transportation problem using Fermatean fuzzy sets and triangular Fermatean fuzzy numbers [64]. These developments have important implications for cost reduction and service improvement in logistics and supply management, particularly in dealing with uncertainty due to unpredictable factors.

The rest of the paper is organized in the following manner. Section 2 is devoted to Coons patches, their construction, twist vectors (MPDs), and the candidate energy functionals which can be used to generate surfaces, such as quasi-minimal, quasi-harmonic, etc. Section 3 is dedicated to finding the optimal twist vectors by ensuring that the gradient of the Dirichlet functional approaches zero. In Section 4, we delve deeper into the optimal twist vectors, which satisfy the condition of the gradient of the harmonic functional vanishing for the same BBCP. For the two cases discussed in Sections 3 and 4, the technique is applied to a BBCP to generate the corresponding quasi-minimal surface for given Hermite blending functions in Section 5. Final remarks and conclusions are given in Section 6.

## 2. A Representation of Bicubically Blended Coons Patch (BBCP)

In this section, a review of basic terminology related to linear blending functions, the rational blending functions, polynomial blending functions such as the Hermite polynomial functions, Coons patches, and BBCPs based on Hermite cubic polynomials is given. We have discussed the role of twist vectors to construct a Coons patch and different techniques which are available for generating these twist vectors. We can utilize the energy functionals, namely, the Dirichlet functional and the quasi-harmonic functional to achieve the accompanying quasi-minimal surface as the extremal of these energy functionals. For this purpose, we need the representation of the BBCP, discussed below. Let us begin our discussion with a Coons patch. A Coons patch (see chapter 22 of ref. [49]) is a type of surface representation used in computer graphics and computer-aided design (CAD) to create smooth surfaces in 3D space. It is commonly used to model complex shapes such as car and aircraft bodies or for blending different surfaces together. Coons patches are formed by interpolating between a set of boundary curves, which can be Bézier or NURBS curves, resulting in a smooth and continuous surface. The method is widely used in CAD and 3D graphics applications to create natural-looking and visually pleasing surfaces. A Coons patch is constrained by four continuous boundary curves  $\mathbf{a}_1(u) = \mathbf{x}(u, 0)$ ,  $\mathbf{a}_2(u) = \mathbf{x}(u, 1)$ ,  $\mathbf{b}_1(v) = \mathbf{x}(0, v)$ , and  $\mathbf{b}_2(v) = \mathbf{x}(1, v)$  for  $u, v \in [0, 1]$ . These curves, along with blending functions  $f_1(u)$ ,  $f_2(u)$ ,  $g_1(v)$ , and  $g_2(v)$ , span the following lofted surfaces:

$$\mathbf{r}_a(u, v) = g_1(v)\mathbf{a}_1(u) + g_2(v)\mathbf{a}_2(u) \quad (1)$$

and

$$\mathbf{r}_b(u, v) = f_1(u)\mathbf{b}_1(v) + f_2(u)\mathbf{b}_2(v) \quad (2)$$

The regular surface  $\mathbf{r}_a$  interpolates only  $a$ -curves and regular surface  $\mathbf{r}_b$  interpolates only  $b$ -curves. For the given corner points  $\mathbf{x}(0, 0)$ ,  $\mathbf{x}(0, 1)$ ,  $\mathbf{x}(1, 0)$ , and  $\mathbf{x}(1, 1)$  connecting the boundary curves, the bivariate interpolant  $\mathbf{r}_{ab}$  is given in the notation

$$\mathbf{r}_{ab} = \begin{pmatrix} f_1(u) & f_2(u) \end{pmatrix} \begin{pmatrix} \mathbf{x}(0, 0) & \mathbf{x}(0, 1) \\ \mathbf{x}(1, 0) & \mathbf{x}(1, 1) \end{pmatrix} \begin{pmatrix} g_1(v) \\ g_2(v) \end{pmatrix}, \quad (3)$$

which helps us to write the known Coons patch

$$\mathbf{x}(u, v) = \mathbf{r}_a(u, v) + \mathbf{r}_b(u, v) - \mathbf{r}_{ab}(u, v), \quad (4)$$

in the following form (by substituting Equations (1), (2) and (3) in Equation (4)):

$$\begin{aligned} \mathbf{x}(u, v) = & (f_1(u) \quad f_2(u)) \begin{pmatrix} \mathbf{x}(0, v) \\ \mathbf{x}(1, v) \end{pmatrix} + (\mathbf{x}(u, 0) \quad \mathbf{x}(u, 1)) \begin{pmatrix} g_1(v) \\ g_2(v) \end{pmatrix} - \\ & (f_1(u) \quad f_2(u)) \begin{pmatrix} \mathbf{x}(0, 0) & \mathbf{x}(0, 1) \\ \mathbf{x}(1, 0) & \mathbf{x}(1, 1) \end{pmatrix} \begin{pmatrix} g_1(v) \\ g_2(v) \end{pmatrix}. \end{aligned} \quad (5)$$

A Coons patch (Equation (5)) is a well-defined surface that can be constructed by the entire information contained in its boundary curves, the four corner points  $\mathbf{x}(0, 0)$ ,  $\mathbf{x}(0, 1)$ ,  $\mathbf{x}(1, 0)$ , and  $\mathbf{x}(1, 1)$  connecting the given prescribed boundary curves, and the auxiliary blending functions  $f_1(u)$ ,  $f_2(u)$ ,  $g_1(v)$ , and  $g_2(v)$ . The surface spanned by such prescribed boundary curves for given corner points for known blending functions is itself called a blending surface and its shape depends not only on the boundary curves but also on different characteristics of blending functions chosen deliberately for some particular aspect of the surface. It can be seen that for  $v = 0$ , the surface  $\mathbf{r}_a(u, v)$  coincides with boundary curve  $\mathbf{x}(u, 0)$ ; for  $v = 1$ , the surface coincides with boundary curve  $\mathbf{x}(u, 1)$ . Similarly, for  $u = 0$  and  $u = 1$ , surface patch  $\mathbf{x}(u, v)$  coincides with boundary curves  $\mathbf{x}(0, v)$  and  $\mathbf{x}(1, v)$ , respectively. The algorithm developed by Ahmad and Masud [19–21] is applicable to a wider class of surfaces. They utilized an ansatz to reduce the area of a target surface and achieve a quasi-minimal surface, specifically for the special case of Equation (5) when all three terms are equal and bounded by four straight lines. The authors used the bilinear interpolation surface as the initial non-minimal surface,

$$\mathbf{x}(u, v) = (f_1(u) \quad f_2(u)) \begin{pmatrix} \mathbf{x}(0, 0) & \mathbf{x}(0, 1) \\ \mathbf{x}(1, 0) & \mathbf{x}(1, 1) \end{pmatrix} \begin{pmatrix} g_1(v) \\ g_2(v) \end{pmatrix}, \quad (6)$$

for the boundary spanned by the lines connected by four corner points  $\mathbf{x}(0, 0)$ ,  $\mathbf{x}(0, 1)$ ,  $\mathbf{x}(1, 0)$ , and  $\mathbf{x}(1, 1)$ , mentioned above, with linear blending functions  $f_1 = 1 - u$ ,  $f_2 = u$ ,  $g_1 = 1 - v$ ,  $g_2 = v$  (see ref. [20]) and the domain of the bilinear interpolant is the unit square and the range is the surface  $\mathbf{x}$  of this unit square. It might be interesting to apply the algorithm to the Coons patches spanned by the blending functions different from the linear ones. A broader class of blending functions could be the following non-linear rational blending functions:

$$f_1(u) = 1 - \frac{u + au^2}{1 + u}, \quad f_2(u) = \frac{u + au^2}{1 + u}, \quad g_1(v) = 1 - \frac{v + av^2}{1 + v}, \quad g_2(v) = \frac{v + av^2}{1 + v}. \quad (7)$$

for  $a \neq 1$ . For  $a = 1$ , the blending functions in Equation (7) reduce to the linear blending functions. The functions  $f_1(u)$ ,  $f_2(u)$ , and  $g_1(v)$ ,  $g_2(v)$  are such that  $f_1(u) + f_2(u)$  and  $g_1(v) + g_2(v)$  are 1, and  $f_1(0) = 1, g_1(v) = 1, f_1(1) = g_1(1) = 0$ . Thus, for  $i, j = 1, 2$ , the above conditions result in

$$\sum_{i=1}^2 f_i(u) = 1, \quad \sum_{i=1}^2 g_i(v) = 1, \quad (8)$$

and

$$f_i(j - 1) = g_i(j - 1) = \delta_{i,j}. \quad (9)$$

Another important class of surfaces, called the bicubically blended Coons patch (BBCP) [49], is a type of surface commonly used in computer graphics and computer-aided design. It is a form of bicubic patch that uses Hermite polynomial segments for interpolation and incorporates information about the four corner points  $\mathbf{x}(0, 0)$ ,  $\mathbf{x}(0, 1)$ ,  $\mathbf{x}(1, 0)$ , and  $\mathbf{x}(1, 1)$ , eight tangent vectors  $\mathbf{x}_u(0, 0)$ ,  $\mathbf{x}_u(1, 0)$ ,  $\mathbf{x}_u(0, 1)$ ,  $\mathbf{x}_u(1, 1)$ ,  $\mathbf{x}_v(0, 0)$ ,  $\mathbf{x}_v(1, 0)$ ,  $\mathbf{x}_v(0, 1)$ ,  $\mathbf{x}_v(1, 1)$  at the given vertices, and four twist vectors  $\mathbf{x}_{uv}(0, 0)$ ,  $\mathbf{x}_{uv}(0, 1)$ ,  $\mathbf{x}_{uv}(1, 0)$ ,

and  $\mathbf{x}_{uv}(1, 1)$ , which are mixed partial derivatives calculated at the respective corner points. The twist vectors are important because they represent how much the surface twists along each of the two principal directions. In the BBCP, the twist vectors are defined as mixed partial derivatives of the surface with respect to both  $u$  and  $v$  at the corner points. This information is used to create a smooth, curved surface that can be used in a variety of applications such as creating car body panels in automotive design, designing airplane wings in aerospace engineering, and creating product designs in industrial design. Overall, the BBCP provides more precise control over the shape of a surface compared to other types of surfaces. By using Hermite polynomial segments and incorporating information about the corner points, tangent vectors, and twist vectors, this approach can create a surface that closely matches the designer's intent. In the particular case, when MPDs are zero, the surface is said to be Ferguson surface. The effect of the non-zero twist vectors at the four corner points of the patch is to make the corner points rounded which are otherwise flattened, thus making the shape of the surface more flexible and giving more control over its shape by adjusting the tangent vectors and the magnitude of twist vectors. For convenience, let us denote the cubic Hermite interpolation functions by  $H_0(w) \equiv H_0^3(w)$ ,  $G_0(w) \equiv H_1^3(w)$ ,  $G_1(w) \equiv H_2^3(w)$ ,  $H_1(w) \equiv H_3^3(w)$ . Then we can work out the two ruled surfaces (the so-called lofted surfaces) bicubically blended by the opposite boundary curves (in  $u$  and  $v$  directions). One of the ruled surfaces can be obtained as the interpolation of the boundary curves  $\mathbf{x}(0, v)$  and  $\mathbf{x}_u(1, v)$  with tangent vectors characterized by  $\mathbf{x}_u(0, v)$ ,  $\mathbf{x}_u(1, v)$ , and the other ruled surface can be achieved by the interpolation of the boundary curves  $\mathbf{x}(u, 0)$ ,  $\mathbf{x}(u, 1)$  with tangent vectors given by  $\mathbf{x}_v(u, 0)$ ,  $\mathbf{x}_v(u, 1)$ . Thus, for one of the ruled surfaces, the blending functions  $H_0(u)$ ,  $G_0(u)$ ,  $G_1(u)$ ,  $H_1(u)$ , cubic Hermite polynomial functions, satisfy the condition in the following manner:

$$\mathbf{x}_c(u, v) = (H_0(u) \quad G_0(u) \quad G_1(u) \quad H_1(u)) \begin{pmatrix} \mathbf{x}(0, v) \\ \mathbf{x}_u(0, v) \\ \mathbf{x}_u(1, v) \\ \mathbf{x}(1, v) \end{pmatrix}, \quad (10)$$

which can be re-written as

$$\mathbf{x}_c(u, v) = H_0(u)\mathbf{x}(0, v) + G_0(u)\mathbf{x}_u(0, v) + G_1(u)\mathbf{x}_u(1, v) + H_1(u)\mathbf{x}(1, v), \quad (11)$$

and for the other ruled surface, blending functions  $H_0(v)$ ,  $G_0(v)$ ,  $G_1(v)$ ,  $H_1(v)$  satisfy the condition

$$\mathbf{x}_d(u, v) = (H_0(v) \quad G_0(v) \quad G_1(v) \quad H_1(v)) \begin{pmatrix} \mathbf{x}(u, 0) \\ \mathbf{x}_v(u, 0) \\ \mathbf{x}_v(u, 1) \\ \mathbf{x}(u, 1) \end{pmatrix}, \quad (12)$$

which can be re-written as

$$\mathbf{x}_d(u, v) = H_0(v)\mathbf{x}(u, 0) + G_0(v)\mathbf{x}_v(u, 0) + G_1(v)\mathbf{x}_v(u, 1) + H_1(v)\mathbf{x}(u, 1). \quad (13)$$

The interpolant at the corner points can be recognized in the same way as it turns up for the Coons patch for the bilinearly blended case. As a result of applying the interpolation technique along both directions, on the corner data only, the product bicubic Hermite interpolant  $\mathbf{x}_{cd}(u, v)$  can be written in the following well-known matrix form:

$$\mathbf{x}_{cd}(u, v) = (H_0(u) \quad G_0(u) \quad G_1(u) \quad H_1(u)) \begin{pmatrix} \mathbf{x}(0, 0) & \mathbf{x}_v(0, 0) & \mathbf{x}_v(0, 1) & \mathbf{x}(0, 1) \\ \mathbf{x}_u(0, 0) & \mathbf{x}_{uv}(0, 0) & \mathbf{x}_{uv}(0, 1) & \mathbf{x}_u(0, 1) \\ \mathbf{x}_u(1, 0) & \mathbf{x}_{uv}(1, 0) & \mathbf{x}_{uv}(1, 1) & \mathbf{x}_u(1, 1) \\ \mathbf{x}(1, 0) & \mathbf{x}_v(1, 0) & \mathbf{x}_v(1, 1) & \mathbf{x}(1, 1) \end{pmatrix} \begin{pmatrix} H_0(v) \\ G_0(v) \\ G_1(v) \\ H_1(v) \end{pmatrix}, \quad (14)$$

The above product bicubic Hermite interpolant  $\mathbf{x}_{cd}(u, v)$  (Equation (14)) is equivalent to its expansion, given below:

$$\begin{aligned} \mathbf{x}_{cd}(u, v) = & H_0(u)H_0(v)\mathbf{x}(0,0) + H_0(u)G_0(v)\mathbf{x}_v(0,0) + H_0(u)G_1(v)\mathbf{x}_v(0,1) + H_0(u)H_1(v)\mathbf{x}(0,1) + \\ & G_0(u)H_0(v)\mathbf{x}_u(0,0) + G_0(u)H_1(v)\mathbf{x}_u(0,1) + G_1(u)H_0(v)\mathbf{x}_u(1,0) + G_1(u)H_1(v)\mathbf{x}_u(1,1) + \\ & H_1(u)H_0(v)\mathbf{x}(1,0) + H_1(u)G_0(v)\mathbf{x}_v(1,0) + H_1(u)G_1(v)\mathbf{x}_v(1,1) + H_1(u)H_1(v)\mathbf{x}(1,1) + \\ & G_0(u)G_0(v)\mathbf{x}_{uv}(0,0) + G_0(u)G_1(v)\mathbf{x}_{uv}(0,1) + G_1(u)G_0(v)\mathbf{x}_{uv}(1,0) + G_1(u)G_1(v)\mathbf{x}_{uv}(1,1). \end{aligned} \tag{15}$$

For the given blending functions, namely the bicubic Hermite polynomial functions satisfying the corner data points, the distinct boundary curves, and the cross-boundary gradients, the general expression for the BBCP can be described as follows:

$$\mathbf{x}(u, v) = \mathbf{x}_c(u, v) + \mathbf{x}_d(u, v) - \mathbf{x}_{cd}(u, v), \tag{16}$$

where  $\mathbf{x}_c, \mathbf{x}_d, \mathbf{x}_{cd}$  are given in Equations (11), (13) and (14). Equation (15) appearing in Equation (16) can be re-arranged in the following convenient notation:

$$\mathbf{x}_{cd}(u, v) = \mathbf{b}(u, v) + \sum_{k,l=0}^1 G_k(u)G_l(v)\mathbf{x}_{uv}(k, l), \tag{17}$$

where  $\mathbf{b}(u, v)$  demonstrates the indicative Ferguson surface, independent of twist vectors; MPDs appear as the part of BBCP, given by

$$\begin{aligned} \mathbf{b}(u, v) = & H_0(u)H_0(v)\mathbf{x}(0,0) + H_0(u)G_0(v)\mathbf{x}_v(0,0) + H_0(u)G_1(v)\mathbf{x}_v(0,1) + H_0(u)H_1(v)\mathbf{x}(0,1) + \\ & G_0(u)H_0(v)\mathbf{x}_u(0,0) + G_0(u)H_1(v)\mathbf{x}_u(0,1) + G_1(u)H_0(v)\mathbf{x}_u(1,0) + G_1(u)H_1(v)\mathbf{x}_u(1,1) + \\ & H_1(u)H_0(v)\mathbf{x}(1,0) + H_1(u)G_0(v)\mathbf{x}_v(1,0) + H_1(u)G_1(v)\mathbf{x}_v(1,1) + H_1(u)H_1(v)\mathbf{x}(1,1), \end{aligned} \tag{18}$$

and the second term involving the summation sign over  $k, l$  represents the following expression:

$$\sum_{k,l=0}^1 G_k(u)G_l(v)\mathbf{x}_{uv}(k, l) = G_0(u)G_0(v)\mathbf{x}_{uv}(0,0) + G_0(u)G_1(v)\mathbf{x}_{uv}(0,1) + G_1(u)G_0(v)\mathbf{x}_{uv}(1,0) + G_1(u)G_1(v)\mathbf{x}_{uv}(1,1). \tag{19}$$

Let us introduce  $\mathbf{c}(u, v)$  as

$$\mathbf{c}(u, v) = \mathbf{x}_c(u, v) + \mathbf{x}_d(u, v) - \mathbf{b}(u, v) \tag{20}$$

to write the BBCP  $\mathbf{x}(u, v)$  given by Equation (16) in the form

$$\mathbf{x}(u, v) = \mathbf{c}(u, v) - \sum_{k,l=0}^1 G_k(u)G_l(v)\mathbf{x}_{uv}(k, l). \tag{21}$$

The form of the BBCP presented above, denoted by  $\mathbf{x}(u, v)$  in Equation (21), is useful for determining the optimal twist vectors through the vanishing condition of the objective functional. It should be noted that  $\mathbf{c}(u, v)$ , which is represented by Equation (20), is included for convenience. However, when expressed in terms of bicubic Hermite polynomial functions, it can be written as

$$\begin{aligned} \mathbf{c}(u, v) = & H_0(u)\mathbf{x}(0, v) + G_0(u)\mathbf{x}_u(0, v) + G_1(u)\mathbf{x}_u(1, v) + H_1(u)\mathbf{x}(1, v) + H_0(v)\mathbf{x}(u, 0) + G_0(v)\mathbf{x}_v(u, 0) + G_1(v) \\ & \times \mathbf{x}_v(u, 1) + H_1(v)\mathbf{x}(u, 1) - H_0(u)H_0(v)\mathbf{x}(0,0) - H_0(u)G_0(v)\mathbf{x}_v(0,0) - H_0(u)G_1(v)\mathbf{x}_v(0,1) - H_0(u) \\ & \times H_1(v)\mathbf{x}(0,1) - G_0(u)H_0(v)\mathbf{x}_u(0,0) - G_0(u)H_1(v)\mathbf{x}_u(0,1) - G_1(u)H_0(v)\mathbf{x}_u(1,0) - G_1(u)H_1(v) \\ & \times \mathbf{x}_u(1,1) - H_1(u)H_0(v)\mathbf{x}(1,0) - H_1(u)G_0(v)\mathbf{x}_v(1,0) - H_1(u)G_1(v)\mathbf{x}_v(1,1) - H_1(u)H_1(v)\mathbf{x}(1,1). \end{aligned} \tag{22}$$

Thus, the bicubically blended Coons patch  $\mathbf{x}(u, v)$  can be expressed as

$$\begin{aligned}
\mathbf{x}(u, v) = & H_0(u)\mathbf{x}(0, v) + G_0(u)\mathbf{x}_u(0, v) + G_1(u)\mathbf{x}_u(1, v) + H_1(u)\mathbf{x}(1, v) + H_0(v)\mathbf{x}(u, 0) + G_0(v)\mathbf{x}_v(u, 0) \\
& + G_1(v)\mathbf{x}_v(u, 1) + H_1(v)\mathbf{x}(u, 1) - H_0(u)H_0(v)\mathbf{x}(0, 0) - H_0(u)G_0(v)\mathbf{x}_v(0, 0) - H_0(u)G_1(v)\mathbf{x}_v(0, 1) \\
& - H_0(u)H_1(v)\mathbf{x}(0, 1) - G_0(u)H_0(v)\mathbf{x}_u(0, 0) - G_0(u)H_1(v)\mathbf{x}_u(0, 1) - G_1(u)H_0(v)\mathbf{x}_u(1, 0) - G_1(u) \\
& \times H_1(v)\mathbf{x}_u(1, 1) - H_1(u)H_0(v)\mathbf{x}(1, 0) - H_1(u)G_0(v)\mathbf{x}_v(1, 0) - H_1(u)G_1(v)\mathbf{x}_v(1, 1) - H_1(u)H_1(v) \\
& \times \mathbf{x}(1, 1)G_0(u)G_0(v)\mathbf{x}_{uv}(0, 0) + G_0(u)G_1(v)\mathbf{x}_{uv}(0, 1) + G_1(u)G_0(v)\mathbf{x}_{uv}(1, 0) + G_1(u)G_1(v)\mathbf{x}_{uv}(1, 1).
\end{aligned} \tag{23}$$

The upper and lower curves in the BBCP (Equation (16)) are

$$\begin{aligned}
\mathbf{x}(u, 0) &= H_0(u)\mathbf{x}(0, 0) + G_0(u)\mathbf{x}_u(0, 0) + G_1(u)\mathbf{x}_u(1, 0) + H_1(u)\mathbf{x}(1, 0), \\
\mathbf{x}(u, 1) &= H_0(u)\mathbf{x}(0, 1) + G_0(u)\mathbf{x}_u(0, 1) + G_1(u)\mathbf{x}_u(1, 1) + H_1(u)\mathbf{x}(1, 1),
\end{aligned} \tag{24}$$

and the left and right boundary curves in the BBCP (Equation (16)) are

$$\begin{aligned}
\mathbf{x}(0, v) &= H_0(v)\mathbf{x}(0, 0) + G_0(v)\mathbf{x}_v(0, 0) + G_1(v)\mathbf{x}_v(0, 1) + H_1(v)\mathbf{x}(0, 1), \\
\mathbf{x}(1, v) &= H_0(v)\mathbf{x}(1, 0) + G_0(v)\mathbf{x}_v(1, 0) + G_1(v)\mathbf{x}_v(1, 1) + H_1(v)\mathbf{x}(1, 1).
\end{aligned} \tag{25}$$

The tangent vectors of the four boundary curves in the BBCP (Equation (16)) can be defined as

$$\begin{aligned}
\mathbf{x}_v(u, 0) &= H_0(u)\mathbf{x}_v(0, 0) + H_1(u)\mathbf{x}_v(1, 0), \\
\mathbf{x}_v(u, 1) &= H_0(u)\mathbf{x}_v(0, 1) + H_1(u)\mathbf{x}_v(1, 1),
\end{aligned} \tag{26}$$

and

$$\begin{aligned}
\mathbf{x}_u(0, v) &= H_0(v)\mathbf{x}_u(0, 0) + H_1(v)\mathbf{x}_u(0, 1), \\
\mathbf{x}_u(1, v) &= H_0(v)\mathbf{x}_u(1, 0) + H_1(v)\mathbf{x}_u(1, 1).
\end{aligned} \tag{27}$$

Finding the suitable twist vectors for a given surface to be calculated or predicted is a challenging job. For this reason, several different schemes have been developed to generate the twist vectors. The twist vectors can be determined by different techniques. These techniques include Forrest's method, bilinear surface formula, and Adini's method. One or the other scheme yields the preferred choice of twist vectors. Forrest's method gives better results than bilinear surface formula, whereas Adini's method gives a better approximation as compared to the other methods [50]. In Forrest's method, the determination of the twist vectors relies on the knowledge of the four corner points of the surface patch, in addition to an additional set of 12 points through which the surface passes. This approach can specifically be applied to the BBCP, as described by Equation (23). The twist vectors can be computed using the bilinear surface formula. The twist vectors can be obtained by differentiating the Coons patch Equation (6) with respect to the surface parameters  $u$  and  $v$  and incorporating the blending functions (linear)  $f_1 = 1 - u$ ,  $f_2 = u$ ,  $g_1 = 1 - v$ , and  $g_2 = v$ ; they are as follows:

$$\mathbf{x}_{uv}(u, v) = \mathbf{x}(0, 0) - \mathbf{x}(0, 1) - \mathbf{x}(1, 0) + \mathbf{x}(1, 1). \tag{28}$$

This equation demonstrates that for a bilinear surface, the twist vector  $\mathbf{x}_{uv}(u, v)$  obtained are invariant across the entire surface patch. Adini's method is recognized for its superior approximation compared to other methods. In this method, four different twist vectors at the four corner points can be determined by using

$$\begin{aligned}
\mathbf{x}_{uv}(0, 0) &= -\mathbf{x}_u(0, 0) + \mathbf{x}_u(0, 1) - \mathbf{x}_v(0, 0) + \mathbf{x}_v(1, 0) - A, \\
\mathbf{x}_{uv}(0, 1) &= -\mathbf{x}_u(0, 0) + \mathbf{x}_u(0, 1) - \mathbf{x}_v(0, 1) + \mathbf{x}_v(1, 1) - A, \\
\mathbf{x}_{uv}(1, 0) &= -\mathbf{x}_u(1, 0) + \mathbf{x}_u(1, 1) - \mathbf{x}_v(0, 0) + \mathbf{x}_v(1, 0) - A, \\
\mathbf{x}_{uv}(1, 1) &= -\mathbf{x}_u(1, 0) + \mathbf{x}_u(1, 1) - \mathbf{x}_v(0, 1) + \mathbf{x}_v(1, 1) - A,
\end{aligned} \tag{29}$$

with  $A$  given by

$$A = \mathbf{x}(0,0) - \mathbf{x}(1,0) - \mathbf{x}(0,1) + \mathbf{x}(1,1), \quad (30)$$

For a more detailed explanation, as mentioned above, the interested reader can refer to Section 16.3 of ref. [49] and Sections (3.3.4) and (3.3.5) of ref. [50]. However, instead of employing any of these techniques directly to generate a surface, we adopt a variational approach in the subsequent sections. We seek the optimal conditions for the twist vectors by determining the vanishing condition of the gradient of the objective functional with respect to the twist vectors at the four corner points, within the context of the BBCP ( $\mathbf{x}(u, v)$ ) given by Equation (16). In the subsequent section, we explore the optimal conditions for the twist vectors by utilizing the Dirichlet functional and the quasi-harmonic functional. By doing so, we can construct the quasi-minimal and quasi-harmonic BBCP, which has applications in various scientific disciplines.

### 3. Optimal Twist Vectors for Bicubically Blended Coons Patch as the Extremal of Dirichlet Functional

The minimization of the area functional

$$J[u] = \int_{\Omega} \sqrt{1 + \|\nabla u(x)\|^2} dx dy, \quad (31)$$

for a hypersurface in  $R^n$  results in the corresponding Euler–Lagrange equation. The solution of this Euler–Lagrange equation is exactly the minimal surface to be determined. The Euler–Lagrange equation is a non-linear second-order partial differential equation. In either case, to find the minimal surface as the surface obtained by optimizing the area functional to find the constraints recognized by the vanishing condition of the gradient of area functional or as the solution of the Euler–Lagrange equation, the non-linearity of the area functional due to the square root of the integrand is a challenging problem for a surface under consideration for the prescribed boundary. In particular, the vanishing condition of gradient of the area functional for a surface given in the form  $u = u(x, y)$  reduces to the Euler–Lagrange equation  $(1 + u_y^2)u_{xx} - 2u_x u_y u_{xy} + (1 + u_x^2)u_{yy} = 0$ , which is a second-order partial differential equation. Known solutions are for some trivial cases rather than its general solution  $z = z(u, v)$ . The analogous linear problem is the minimization of the Dirichlet energy functional

$$D(u) = \frac{1}{2} \int_{\Omega} \|\nabla u\|^2 dx dy, \quad (32)$$

where the gradient vector field of function  $u$  is denoted by  $\nabla u : \Omega \rightarrow R^n$ . The Dirichlet energy integral is obviously a non-negative quantity for every function  $u$ . The corresponding Euler–Lagrange equation is  $\Delta u = 0$ , which represents the Laplace equation in 2D. Therefore, harmonic functions are the critical points of the Dirichlet variational functional. A regular parameterized surface  $\mathbf{x} : U \subset R^2 \rightarrow V \subset R^3$ , where  $U$  is an open set in  $R^2$  and  $V$  is a subset of  $R^3$ , is considered a surface  $\mathbf{x} = \mathbf{x}(u, v)$ ,  $(u, v) \in U$ , which aims to minimize its area locally. This minimization of area is equivalent to achieving zero mean curvature,

$$H(u, v) = \frac{1}{2} \frac{Eg - 2Ff + Ge}{EG - F^2}, \quad (33)$$

for every possible parametrization of the surface, which is a direct outcome of minimizing the area functional,

$$A(\mathbf{x}) = \int_R \|\mathbf{x}_u \wedge \mathbf{x}_v\| dudv = \int_R (EG - F^2)^{1/2} dudv, \quad (34)$$

where  $E = \langle \mathbf{x}_u, \mathbf{x}_u \rangle$ ,  $F = \langle \mathbf{x}_u, \mathbf{x}_v \rangle$  and  $G = \langle \mathbf{x}_v, \mathbf{x}_v \rangle$  are coefficients of the quadratic form

$$I(u, v) = \langle d\mathbf{x}(u, v), d\mathbf{x}(u, v) \rangle, \quad (35)$$

and the mapping of vectors  $(du, dv)$  onto

$$d\mathbf{x}(u, v) = \mathbf{x}_u du + \mathbf{x}_v dv \quad (36)$$

is a one-to-one linear transformation that lies in the tangent plane. This transformation corresponds to the first fundamental form, which is a quadratic form given by Equation (35). The first fundamental form is commonly expressed as

$$ds^2 = E(u, v)du^2 + 2F(u, v)dudv + G(u, v)dv^2, \quad (37)$$

for the surface  $\mathbf{x}(u, v)$ . The minimization of the Dirichlet energy functional (32), as mentioned above, serves as the analogous linear problem for minimizing the area functional (Equation (34)), which for a regular parameterized surface  $\mathbf{x}(u, v)$  can be written in the form

$$D(\mathbf{x}) = \frac{1}{2} \int_{\mathcal{R}} (E(u, v) + G(u, v))dudv = \frac{1}{2} \int_{\mathcal{R}} (\|\mathbf{x}_u\|^2 + \|\mathbf{x}_v\|^2)dudv. \quad (38)$$

The Dirichlet functional (38) can be related to the area functional (34) by recalling that the following inequality relation,

$$(EG - F^2)^{1/2} \leq (EG)^{1/2} \leq \frac{E + G}{2}, \quad (39)$$

implies that  $A(\mathbf{x}) \leq D(\mathbf{x})$  for a given surface and the equality occurs only in the case of isothermal charts, i.e., for  $E = G$  and  $F = 0$ . The Dirichlet functional (38), being the linear analogue of area function (34), can be used conveniently to obtain the quasi-minimal surface as the solution of the vanishing condition of the gradient of the Dirichlet functional. Our target surface is the bicubically blended Coons patch (BBCP)  $\mathbf{x}(u, v)$  given by Equation (21), and we wish to find the quasi-minimal BBCP as the solution of the variational minimization of the Dirichlet functional (38). For this purpose, we find  $\partial D(\mathbf{x})/\partial \mathbf{x}_{uv}(m, n)$ , the gradient of the Dirichlet functional (38) w.r.t. the twist vectors  $\mathbf{x}_{uv}(m, n)$  for  $m, n = 0, 1$  and then the constraints are obtained for the vanishing condition, i.e.,  $\partial D(\mathbf{x})/\partial \mathbf{x}_{uv}(m, n) = 0$ , for the BBCP  $\mathbf{x}(u, v)$ , given by Equation (21). For this purpose, we proceed as follows.

Let us denote the partial derivatives of  $\mathbf{x}(u, v)$  w.r.t. the surface parameters  $u, v$  of the BBCP Equation (21) by  $\mathbf{x}_u(u, v)$  and  $\mathbf{x}_v(u, v)$ , respectively. They are

$$\begin{aligned} \mathbf{x}_u(u, v) &= \mathbf{c}_u(u, v) - \sum_{k,l=0}^1 (G_k(u))' G_l(v) \mathbf{x}_{uv}(k, l), \\ \mathbf{x}_v(u, v) &= \mathbf{c}_v(u, v) - \sum_{k,l=0}^1 G_k(u) (G_l(v))' \mathbf{x}_{uv}(k, l). \end{aligned} \quad (40)$$

We then substitute the values of these partial derivatives  $\mathbf{x}_u(u, v)$  and  $\mathbf{x}_v(u, v)$  from the above Equation (40) in Equation (38) to obtain

$$D(\mathbf{x}) = D_1(\mathbf{x}) + D_2(\mathbf{x}), \quad (41)$$

where

$$D_1(\mathbf{x}) = \frac{1}{2} \int_{\mathcal{R}} \|\mathbf{c}_u(u, v) - \sum_{k,l=0}^1 (G_k(u))' G_l(v) \mathbf{x}_{uv}(k, l)\|^2 dudv, \quad (42)$$

and

$$D_2(\mathbf{x}) = \frac{1}{2} \int_{\mathcal{R}} \|\mathbf{c}_v(u, v) - \sum_{k,l=0}^1 G_k(u)(G_l(v))' \mathbf{x}_{uv}(k, l)\|^2 dudv, \tag{43}$$

where  $(G_k(u))'$  and  $(G_l(v))'$ , showing up in the above Equations (42) and(43), denote the derivatives of the  $G_k(u)$  and  $G_l(v)$  w.r.t. the surface parameters  $u$  and  $v$ , respectively, and the summation terms in the above equations are

$$\begin{aligned} \sum_{k,l=0}^1 (G_k(u))' G_l(v) \mathbf{x}_{uv}(k, l) &= (G_0(u))' G_0(v) \mathbf{x}_{uv}(0, 0) + (G_0(u))' G_1(v) \mathbf{x}_{uv}(0, 1) \\ &\quad + (G_1(u))' G_0(v) \mathbf{x}_{uv}(1, 0) + (G_1(u))' G_1(v) \mathbf{x}_{uv}(1, 1), \tag{44} \\ \sum_{k,l=0}^1 G_k(u) (G_l(v))' \mathbf{x}_{uv}(k, l) &= G_0(u) (G_0(v))' \mathbf{x}_{uv}(0, 0) + G_0(u) (G_1(v))' \mathbf{x}_{uv}(0, 1) \\ &\quad + G_1(u) (G_0(v))' \mathbf{x}_{uv}(1, 0) + G_1(u) (G_1(v))' \mathbf{x}_{uv}(1, 1). \end{aligned}$$

Let us denote by  $\partial_{\mathbf{x}_{uv}(s,t)} D_1(\mathbf{x})$  and  $\partial_{\mathbf{x}_{uv}(s,t)} D_2(\mathbf{x})$  the partial derivatives of Equations (42) and (43) w.r.t. MPDs  $\mathbf{x}_{uv}(s, t)$ , which can be expressed in the form

$$\partial_{\mathbf{x}_{uv}(s,t)} D_1(\mathbf{x}) = - \int_{\mathcal{R}} (G_s(u))' G_t(v) \langle \mathbf{c}_u(u, v), e^a \rangle dudv + \sum_{k,l=0}^1 \int_{\mathcal{R}} (G_s(u))' G_t(v) (G_k(u))' G_l(v) \langle \mathbf{x}_{uv}(k, l), e^a \rangle dudv, \tag{45}$$

and

$$\partial_{\mathbf{x}_{uv}(s,t)} D_2(\mathbf{x}) = - \int_{\mathcal{R}} G_s(u) (G_t(v))' \langle \mathbf{c}_v(u, v), e^a \rangle dudv + \sum_{k,l=0}^1 \int_{\mathcal{R}} G_s(u) (G_t(v))' G_k(u) (G_l(v))' \langle \mathbf{x}_{uv}(k, l), e^a \rangle dudv. \tag{46}$$

Thus, the vanishing condition for the gradient  $\partial_{\mathbf{x}_{uv}(s,t)} D(\mathbf{x}) = \partial_{\mathbf{x}_{uv}(s,t)} D_1(\mathbf{x}) + \partial_{\mathbf{x}_{uv}(s,t)} D_2(\mathbf{x})$  of the Dirichlet functional (41) w.r.t. the MPDs  $\mathbf{x}_{uv}(s, t)$  for  $s, t \in \{0, 1\}$  along with Equations (45) and (46) can be written in the form

$$\begin{aligned} &\sum_{k,l=0}^1 \left( \int_{\mathcal{R}} \left( (G_s(u))' G_t(v) (G_k(u))' G_l(v) + G_s(u) (G_t(v))' G_k(u) (G_l(v))' \right) dudv \right) \langle \mathbf{x}_{uv}(k, l), e^a \rangle \\ &= \left\langle \int_{\mathcal{R}} (G_s(u))' G_t(v) \mathbf{c}_u(u, v) + G_s(u) (G_t(v))' \mathbf{c}_v(u, v) dudv, e^a \right\rangle. \end{aligned} \tag{47}$$

For convenience, let us identify the integrals by

$$P(k, l, s, t) = \int_{\mathcal{R}} \left( (G_s(u))' G_t(v) (G_k(u))' G_l(v) + G_s(u) (G_t(v))' G_k(u) (G_l(v))' \right) dudv, \tag{48}$$

and

$$\mathbf{Q}(s, t) = \int_{\mathcal{R}} (G_s(u))' G_t(v) \mathbf{c}_u(u, v) + G_s(u) (G_t(v))' \mathbf{c}_v(u, v) dudv, \tag{49}$$

which helps us to write the vanishing condition specified by Equation (47) in the following precise form:

$$\sum_{k,l=0}^1 P(k, l, s, t) \mathbf{x}_{uv}(k, l) = \mathbf{Q}(s, t). \tag{50}$$

For  $s, t \in \{0, 1\}$ , Equation (50) splits up into the following four equations:

$$\begin{aligned} P(0, 0, 0, 0) \mathbf{x}_{uv}(0, 0) + P(0, 1, 0, 0) \mathbf{x}_{uv}(0, 1) + P(1, 0, 0, 0) \mathbf{x}_{uv}(1, 0) + P(1, 1, 0, 0) \mathbf{x}_{uv}(1, 1) &= \mathbf{Q}(0, 0), \\ P(0, 0, 0, 1) \mathbf{x}_{uv}(0, 0) + P(0, 1, 0, 1) \mathbf{x}_{uv}(0, 1) + P(1, 0, 0, 1) \mathbf{x}_{uv}(1, 0) + P(1, 1, 0, 1) \mathbf{x}_{uv}(1, 1) &= \mathbf{Q}(0, 1), \\ P(0, 0, 1, 0) \mathbf{x}_{uv}(0, 0) + P(0, 1, 1, 0) \mathbf{x}_{uv}(0, 1) + P(1, 0, 1, 0) \mathbf{x}_{uv}(1, 0) + P(1, 1, 1, 0) \mathbf{x}_{uv}(1, 1) &= \mathbf{Q}(1, 0), \\ P(0, 0, 1, 1) \mathbf{x}_{uv}(0, 0) + P(0, 1, 1, 1) \mathbf{x}_{uv}(0, 1) + P(1, 0, 1, 1) \mathbf{x}_{uv}(1, 0) + P(1, 1, 1, 1) \mathbf{x}_{uv}(1, 1) &= \mathbf{Q}(1, 1), \end{aligned} \tag{51}$$

Equivalently, the system of Equations (51) can be expressed in the following matrix form:

$$\begin{pmatrix} P(0,0,0,0) & P(0,1,0,0) & P(1,0,0,0) & P(1,1,0,0) \\ P(0,0,0,1) & P(0,1,0,1) & P(1,0,0,1) & P(1,1,0,1) \\ P(0,0,1,0) & P(0,1,1,0) & P(1,0,1,0) & P(1,1,1,0) \\ P(0,0,1,1) & P(0,1,1,1) & P(1,0,1,1) & P(1,1,1,1) \end{pmatrix} \begin{pmatrix} x_{uv}^a(0,0) \\ x_{uv}^a(0,1) \\ x_{uv}^a(1,0) \\ x_{uv}^a(1,1) \end{pmatrix} = \begin{pmatrix} Q^a(0,0) \\ Q^a(0,1) \\ Q^a(1,0) \\ Q^a(1,1) \end{pmatrix}. \tag{52}$$

The simultaneous solution of the above four Equations (51) (or the matrix form (52) for  $a = 1, 2, 3$ ,  $\mathbf{x}_{uv}(k, l) = (x_{uv}^a(k, l)) = (x_{uv}^1(k, l), x_{uv}^2(k, l), x_{uv}^3(k, l))$ ) for the unknown twist vectors  $\mathbf{x}_{uv}(0, 0), \mathbf{x}_{uv}(0, 1), \mathbf{x}_{uv}(1, 0)$ , and  $\mathbf{x}_{uv}(1, 1)$  gives us these twist vectors in terms of  $P(k, l, s, t)$  and  $\mathbf{Q}(s, t)$ . The integrals  $P(k, l, s, t)$  and  $\mathbf{Q}(s, t)$  are given by the Equations (48) and (49) for  $k, l, s, t \in \{0, 1\}$ . For the twist vectors  $\mathbf{x}_{uv}(0, 0), \mathbf{x}_{uv}(0, 1), \mathbf{x}_{uv}(1, 0)$  and  $\mathbf{x}_{uv}(1, 1)$ , computed in this way, we can find the quasi-minimal BBCP corresponding to the BBCP Equation (21) as the extremal of Dirichlet functional (38).

#### 4. Optimal Twist Vectors for Bicubically Blended Coons Patch as the Extremal of Quasi-Harmonic Functional

In this section, we shall find the optimal twist vectors  $\mathbf{x}_{uv}(m, n)$  for  $m, n = 0, 1$  for the BBCP,  $\mathbf{x}(u, v)$  (Equation (21)) obtained from the vanishing condition of quasi-harmonic functional

$$Q(u, v) = \int_R \|\mathbf{x}_{uu} + \mathbf{x}_{vv}\|^2 dudv, \tag{53}$$

where  $\mathbf{x}_{uu}(u, v)$  and  $\mathbf{x}_{vv}(u, v)$  are second-order partial derivatives of the surface  $\mathbf{x}(u, v)$  w.r.t the surface parameters  $u, v$ . We partially differentiate Equation (21) w.r.t the surface parameters  $u, v$  to find

$$\mathbf{x}_{uu}(u, v) = \mathbf{c}_{uu}(u, v) - \sum_{k,l=0}^1 (G_k(u))'' G_l(v) \mathbf{x}_{uv}(k, l), \tag{54}$$

$$\mathbf{x}_{vv}(u, v) = \mathbf{c}_{vv}(u, v) - \sum_{k,l=0}^1 G_k(u) (G_l(v))'' \mathbf{x}_{uv}(k, l), \tag{55}$$

and the sum of the partial derivatives (Equations (54) and (55)) of the surface  $\mathbf{x}(u, v)$  (Equation (21)) w.r.t the surface parameters  $u, v$  can be written as

$$\mathbf{x}_{uu}(u, v) + \mathbf{x}_{vv}(u, v) = \mathbf{c}_{uu}(u, v) + \mathbf{c}_{vv}(u, v) - \sum_{k,l=0}^1 \left( (G_k(u))'' G_l(v) + G_k(u) (G_l(v))'' \right) \mathbf{x}_{uv}(k, l). \tag{56}$$

The vanishing condition for gradient  $\partial_{\mathbf{x}_{uv}(s,t)} Q(u, v)$  of the quasi-harmonic functional (53) w.r.t. the MPDs  $\mathbf{x}_{uv}(s, t)$  for  $s, t \in \{0, 1\}$  of the surface  $\mathbf{x}(u, v)$  (Equation (21)),

$$\int_R \left\langle (\mathbf{x}_{uu} + \mathbf{x}_{vv}), \frac{\partial}{\partial \mathbf{x}_{uv}(s, t)} (\mathbf{x}_{uu} + \mathbf{x}_{vv}) \right\rangle dudv = 0, \tag{57}$$

along with Equation (56)

$$\int_R \left( (\mathbf{c}_{uu}(u, v) + \mathbf{c}_{vv}(u, v)) \left( (G_s(u))'' G_t(v) + G_s(u) (G_t(v))'' \right) - \sum_{k,l=0}^1 \left( (G_k(u))'' \times \right. \right. \\ \left. \left. G_l(v) + G_k(u) (G_l(v))'' \right) \left( (G_s(u))'' G_t(v) + G_s(u) (G_t(v))'' \right) \mathbf{x}_{uv}(k, l) \right) dudv = 0, \tag{58}$$

takes the following form:

$$\begin{aligned} & \sum_{k,l=0}^1 \int_R \left( (G_k(u))'' G_l(v) + G_k(u) (G_l(v))'' \right) \left( (G_s(u))'' G_t(v) + G_s(u) (G_t(v))'' \right) \mathbf{x}_{uv}(k,l) dudv \\ &= \int_R (\mathbf{c}_{uu}(u,v) + \mathbf{c}_{vv}(u,v)) \left( (G_s(u))'' G_t(v) + G_s(u) (G_t(v))'' \right) dudv. \end{aligned} \tag{59}$$

Let us denote the corresponding integrals in Equation (59) by

$$Y(k,l,s,t) = \int_R \left( (G_k(u))'' G_l(v) + G_k(u) (G_l(v))'' \right) \left( (G_s(u))'' G_t(v) + G_s(u) (G_t(v))'' \right) dudv, \tag{60}$$

and

$$\mathbf{W}(s,t) = \int_R (\mathbf{c}_{uu}(u,v) + \mathbf{c}_{vv}(u,v)) \left( (G_s(u))'' G_t(v) + G_s(u) (G_t(v))'' \right) dudv, \tag{61}$$

to write the vanishing condition (59)

$$\sum_{k,l=0}^1 Y(k,l,s,t) \mathbf{x}_{uv}(k,l) = \mathbf{W}(s,t). \tag{62}$$

Equation (62), an obvious linear combination of MPDs  $\mathbf{x}_{uv}(k,l)$  for  $k,l,s,t \in \{0,1\}$  where  $k,l$  appear as dummy indices and  $s,t$  as the free indices, can be expressed as

$$\begin{aligned} Y(0,0,0,0) \mathbf{x}_{uv}(0,0) + Y(0,1,0,0) \mathbf{x}_{uv}(0,1) + Y(1,0,0,0) \mathbf{x}_{uv}(1,0) + Y(1,1,0,0) \mathbf{x}_{uv}(1,1) &= \mathbf{W}(0,0) \\ Y(0,0,0,1) \mathbf{x}_{uv}(0,0) + Y(0,1,0,1) \mathbf{x}_{uv}(0,1) + Y(1,0,0,1) \mathbf{x}_{uv}(1,0) + Y(1,1,0,1) \mathbf{x}_{uv}(1,1) &= \mathbf{W}(0,1) \\ Y(0,0,1,0) \mathbf{x}_{uv}(0,0) + Y(0,1,1,0) \mathbf{x}_{uv}(0,1) + Y(1,0,1,0) \mathbf{x}_{uv}(1,0) + Y(1,1,1,0) \mathbf{x}_{uv}(1,1) &= \mathbf{W}(1,0) \\ Y(0,0,1,1) \mathbf{x}_{uv}(0,0) + Y(0,1,1,1) \mathbf{x}_{uv}(0,1) + Y(1,0,1,1) \mathbf{x}_{uv}(1,0) + Y(1,1,1,1) \mathbf{x}_{uv}(1,1) &= \mathbf{W}(1,1) \end{aligned} \tag{63}$$

Equivalently, the system of Equations (63) can be written in the matrix form

$$\begin{pmatrix} Y(0,0,0,0) & Y(0,1,0,0) & Y(1,0,0,0) & Y(1,1,0,0) \\ Y(0,0,0,1) & Y(0,1,0,1) & Y(1,0,0,1) & Y(1,1,0,1) \\ Y(0,0,1,0) & Y(0,1,1,0) & Y(1,0,1,0) & Y(1,1,1,0) \\ Y(0,0,1,1) & Y(0,1,1,1) & Y(1,0,1,1) & Y(1,1,1,1) \end{pmatrix} \begin{pmatrix} x_{uv}^a(0,0) \\ x_{uv}^a(0,1) \\ x_{uv}^a(1,0) \\ x_{uv}^a(1,1) \end{pmatrix} = \begin{pmatrix} W^a(0,0) \\ W^a(0,1) \\ W^a(1,0) \\ W^a(1,1) \end{pmatrix}, \tag{64}$$

with the usual matrix notation for

$$Y(k,l,s,t) = \begin{pmatrix} Y(0,0,0,0) & Y(0,1,0,0) & Y(1,0,0,0) & Y(1,1,0,0) \\ Y(0,0,0,1) & Y(0,1,0,1) & Y(1,0,0,1) & Y(1,1,0,1) \\ Y(0,0,1,0) & Y(0,1,1,0) & Y(1,0,1,0) & Y(1,1,1,0) \\ Y(0,0,1,1) & Y(0,1,1,1) & Y(1,0,1,1) & Y(1,1,1,1) \end{pmatrix}, x_{uv}^a(k,l) = \begin{pmatrix} x_{uv}^a(0,0) \\ x_{uv}^a(0,1) \\ x_{uv}^a(1,0) \\ x_{uv}^a(1,1) \end{pmatrix}, W^a(s,t) = \begin{pmatrix} W^a(0,0) \\ W^a(0,1) \\ W^a(1,0) \\ W^a(1,1) \end{pmatrix} \tag{65}$$

By solving the above four Equations (63) simultaneously (or in matrix form (64) for  $a = 1, 2, 3$ ,  $\mathbf{x}_{uv}(k,l) = (x_{uv}^a(k,l)) = (x_{uv}^1(k,l), x_{uv}^2(k,l), x_{uv}^3(k,l))$ ), we can find all the twist vectors  $\mathbf{x}_{uv}(0,0), \mathbf{x}_{uv}(0,1), \mathbf{x}_{uv}(1,0)$  and  $\mathbf{x}_{uv}(1,1)$  in terms of  $Y(k,l,s,t)$  and  $\mathbf{W}(s,t)$ . The integrals  $Y(k,l,s,t)$  and  $\mathbf{W}(s,t)$  are given by (60) and (61) for  $k,l,s,t \in \{0,1\}$ . By computing the twist vectors  $\mathbf{x}_{uv}(0,0), \mathbf{x}_{uv}(0,1), \mathbf{x}_{uv}(1,0)$ , and  $\mathbf{x}_{uv}(1,1)$  in this manner, the BBCP equation (21) represents an extremal quasi-harmonic BBCP of the quasi-harmonic functional (53).

### 5. Application: Coons Patch (BBCP) Spanned by Hermite Cubic Polynomials

In this section, we illustrate the technique developed in the above section by applying it to a bicubically blended Coons patch. For instance, we can construct a Coons patch (Equation (5)) by replacing the blending functions (say  $f_1(u), f_2(u)$ , and  $g_1(v), g_2(v)$ ) with

the Hermite cubic polynomials (denoted by  $H_0(u)$ ,  $H_1(u)$ , and  $H_0(v)$ ,  $H_1(v)$ ) that satisfy the Coons patch condition (8) that  $H_0(u) + H_1(u) = 1$ . From this deliberately chosen Coons patch, we can calculate the cross-boundary tangent vectors at  $u = 0$ ,  $u = 1$ ,  $v = 0$ ,  $v = 1$  for cross-boundary tangents and the twist vectors at the boundary points  $(0,0)$ ,  $(1,0)$ ,  $(1,1)$ ,  $(0,1)$  by finding the first-order and second-order partial derivatives of the same Coons patch. This gives us the cross-boundary tangent vectors and mixed partial derivatives at the already known boundary points  $(u, v) \in \{(0,0), (1,0), (1,1), (0,1)\}$  for the ruled surfaces (10), (12) and the product bicubic Hermite interpolant (14) for the BBCP in the form (23). Let us start by writing the Hermite cubic polynomials

$$H_0(u) = 2u^3 - 3u^2 + 1, G_0(u) = u^3 - 2u^2 + u, G_1(u) = u^3 - u^2, H_1(u) = 3u^2 - 2u^3, \quad (66)$$

the boundary curves

$$\mathbf{x}(u, 0) = (u, 0, u - u^2), \mathbf{x}(u, 1) = (u^3, 1, u^2 - u), \mathbf{x}(0, v) = (0, v^2, v - v^2), \mathbf{x}(1, v) = (1, v^2, v - v^3), \quad (67)$$

and the corner points

$$\mathbf{x}(0, 0) = (0, 0, 0), \mathbf{x}(0, 1) = (0, 1, 0), \mathbf{x}(1, 0) = (1, 0, 0), \mathbf{x}(1, 1) = (1, 1, 0), \quad (68)$$

which, when substituted into Equation (5), gives us the following expression for the Coons patch:

$$\begin{aligned} x(u, v) &= -2u^3v^3 + 3u^3v^2 + 2uv^3 - 3uv^2 + u, & y(u, v) &= v^2, \\ z(u, v) &= 2u^3v^3 - 2u^3v^2 - 7u^2v^3 + 9u^2v^2 - u^2 + 4uv^3 - 6uv^2 + u - v^2 + v. \end{aligned} \quad (69)$$

The boundary curves for the Coons patch (69) are given by (67), and a graphical representation of these boundary curves for the Coons patch (69) is shown in Figure 1. The Coons patch (69) itself, with the prescribed boundary curves (67), is shown in Figure 2.

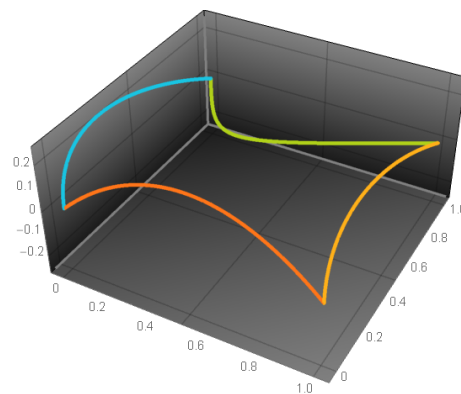


**Figure 1.** Prescribed boundary given by Equation (67) shown for the Coons Patch Equation (69).

The Coons patch (69) provides a useful framework for constructing surfaces in computer graphics and geometric modeling. The quality of the resulting surface may be limited by the flattened appearance that occurs when identical twist vectors are used at all four corners. For instance, it can be immediately seen for the bilinearly blended surface given by Equation (6) with blending functions defined by  $f_1 = 1 - u$ ,  $f_2 = u$ ,  $g_1 = 1 - v$ , and  $g_2 = v$  (ref. [20]) (the functions are linear) that the twist vectors for this surface are identical and they are  $\mathbf{x}_{uv}(0,0) = \mathbf{x}_{uv}(0,1) = \mathbf{x}_{uv}(1,0) = \mathbf{x}_{uv}(1,1) = (0,0,3)$  over the domain of the unit square for the bilinear interpolant. To address this issue, this study proposes a method of calculating different twist vectors at each corner of the surface, resulting in a more rounded surface that better approximates the underlying geometry. The effectiveness of this approach depends on the roundedness of the Coons patch and the use of mixed partial derivatives.

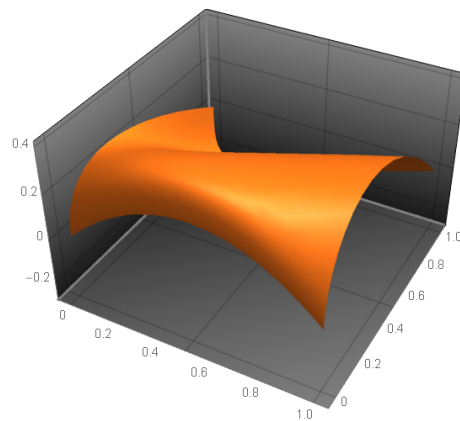


**Figure 2.** Coons patch Equation (69) for the prescribed boundary.

In addition to the improved visual appearance of the surface, optimizing the twist vectors also has implications for the efficiency of the Coons patch. From Coons patch (69), we can obtain cross-boundary tangent vectors at  $u = 0, u = 1, v = 0, v = 1$  and mixed partial derivatives at corner points  $(0, 0), (1, 0), (1, 1), (0, 1)$  for the ruled surfaces (10), (12) and the product bicubic Hermite interpolant (14) for the BBCP (23). The resulting BBCP (23) for this explicit choice of boundary curves and blending functions reduces to a more efficient and higher-quality representation of the underlying geometry, compared to using identical twist vectors at all four corners. For this explicit choice of boundary curves and blending functions, the bicubically blended Coons patch (23) can be represented by

$$\begin{aligned} x(u, v) &= 4u^3v^3 - 3u^3v^2 - 6u^2v^3 + 6u^2v^2 + 2uv^3 - 3uv^2 + u, \\ y(u, v) &= v^2, \\ z(u, v) &= 2u^3v^3 + 2u^3v^2 - 4u^3v - 7u^2v^3 + 3u^2v^2 + 6u^2v - u^2 + 4uv^3 - 4uv^2 - 2uv + u - v^2 + v, \end{aligned} \quad (70)$$

shown in Figure 3.

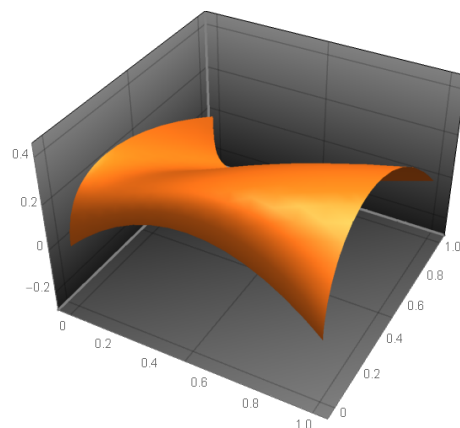


**Figure 3.** Bicubically blended Coons patch Equation (70) for the prescribed boundary.

The mean curvature  $H$  of a locally parameterized surface is usually written in the form

$$H(u, v) = H_n/2w, \quad (71)$$

where

$$H_n(u, v) = Ge - 2Ff + Eg, w(u, v) = EG - F^2, \quad (72)$$

and the Gaussian curvature

$$K(u, v) = (eg - f^2)/w, \quad (73)$$

where  $E, F, G, e, f, g$  denote the fundamental coefficients of the surface given by

$$E = \langle \mathbf{x}_u, \mathbf{x}_u \rangle, \quad F = \langle \mathbf{x}_u, \mathbf{x}_v \rangle, \quad G = \langle \mathbf{x}_v, \mathbf{x}_v \rangle, \quad e = \langle \mathbf{N}, \mathbf{x}_{uu} \rangle, \quad f = \langle \mathbf{N}, \mathbf{x}_{uv} \rangle, \quad g = \langle \mathbf{N}, \mathbf{x}_{vv} \rangle, \quad (74)$$

with the unit normal to the surface  $\mathbf{x}(u, v)$  defined by

$$\mathbf{N}(u, v) = \frac{\mathbf{x}_u \times \mathbf{x}_v}{|\mathbf{x}_u \times \mathbf{x}_v|}, \quad (75)$$

The mean curvature (71) for a locally parameterized minimal surface should identically be zero, or identically the numerator  $H_n$  (Equation (72)) of the mean curvature (71) is zero. The fundamental coefficients can be found in Appendix A (Equations (A1)–(A6)), with  $w = EG - F^2$  in Equation (A7). Additionally, the numerator of the mean curvature of the BBCP, denoted by  $H_n$ , is provided in Appendix A (Equation (A8)). The numerator  $H_n$  of the mean curvature of the BBCP is shown in Figure 4.

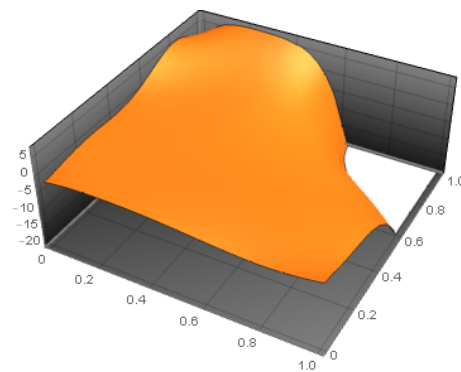


**Figure 4.** Numerator  $H_n$  (given in Appendix A, Equation (A8)) of the mean curvature of the Bicubically blended Coons patch.

The expression for the numerator of the Gaussian curvature appears in Appendix A (Equation (A9)) and is shown in the Figure 5.

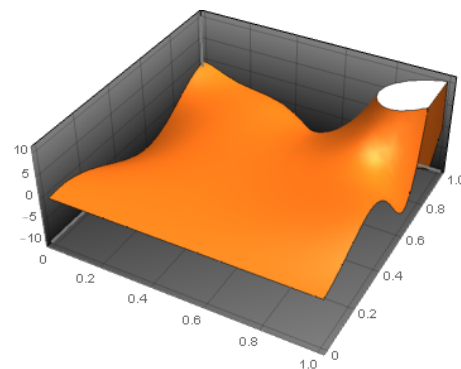


**Figure 5.** Numerator of the Gaussian curvature (see Appendix A, Equation (A9)) of the bicubically blended Coons patch.

For further illustration of the technique, we find the MPDs as the solution of the simultaneous system of equations Equation (62) as the extremal of the quasi-harmonic functional. These MPDs, when substituted into the BBCP given by the Equation (70), give us the extremal BBCP of quasi-harmonic functional. We compute the second-order partial derivatives Equations (54) and (55) in order to find  $\mathbf{c}_{uu}(u, v) + \mathbf{c}_{vv}(u, v)$  from the following expression for  $\mathbf{c}(u, v) = (c^1(u, v), c^2(u, v), c^3(u, v))$  for

$$\begin{aligned}
 c^1(u, v) &= -96u^{11}v^6 + 144u^{11}v^5 - 54u^{11}v^4 + 480u^{10}v^6 - 780u^{10}v^5 + 315u^{10}v^4 - 952u^9v^6 + 1698u^9v^5 - 747u^9v^4 - \\
 &32u^9v^3 + 24u^9v^2 + 952u^8v^6 - 1890u^8v^5 + 918u^8v^4 + 116u^8v^3 - 96u^8v^2 - 500u^7v^6 + 1122u^7v^5 - 612 \times \\
 &u^7v^4 - 146u^7v^3 + 138u^7v^2 - 2u^7 + 128u^6v^6 - 330u^6v^5 + 207u^6v^4 + 82u^6v^3 - 90u^6v^2 + 5u^6 - 12u^5v^6 + \\
 &36u^5v^5 - 27u^5v^4 - 48u^5v^3 + 48u^5v^2 - 3u^5 + 46u^4v^3 - 45u^4v^2 + 2u^4 - 16u^3v^3 + 21u^3v^2 - 4u^3 - 4u^2v^3 + \\
 &3u^2v^2 + u^2 + 2uv^3 - 3uv^2 + u \\
 c^2(u, v) &= 2u^3v^2 - 3u^2v^2 + v^2 \\
 c^3(u, v) &= -24u^{11}v^6 - 48u^{11}v^5 + 72u^{11}v^4 + 96u^{11}v^3 - 96u^{11}v^2 + 200u^{10}v^6 + 200u^{10}v^5 - 640u^{10}v^4 - 220u^{10}v^3 + \quad (76) \\
 &500u^{10}v^2 - 40u^{10}v - 646u^9v^6 - 104u^9v^5 + 1782u^9v^4 - 218u^9v^3 - 994u^9v^2 + 180u^9v - 4u^9 + 1028 \times \\
 &u^8v^6 - 528u^8v^5 - 2156u^8v^4 + 1020u^8v^3 + 944u^8v^2 - 308u^8v + 16u^8 - 842u^7v^6 + 858u^7v^5 + 1216 \times \\
 &u^7v^4 - 1029u^7v^3 - 455u^7v^2 + 252u^7v - 23u^7 + 332u^6v^6 - 424u^6v^5 - 350u^6v^4 + 413u^6v^3 + 141u^6 \times \\
 &v^2 - 112u^6v + 14u^6 - 48u^5v^6 + 34u^5v^5 + 100u^5v^4 - 90u^5v^3 - 51u^5v^2 + 59u^5v - 5u^5 + 12u^4v^5 - 24u^4 \times \\
 &v^4 + 55u^4v^3 - 8u^4v^2 - 49u^4v + 7u^4 - 28u^3v^3 + 22u^3v^2 + 18u^3v - 6u^3 - 3u^2v^3 + 2u^2v^2 + u^2v + 4uv^3 - \\
 &4uv^2 - 2uv + u - v^2 + v.
 \end{aligned}$$

We substitute the above expression for  $c(u, v)$  in Equation (61) and determine the integrals Equation (60) and Equation (61) required for the vanishing condition Equation (62). The matrix  $Y(k, l, s, t)$  of the integral coefficients Equation (65) for the quasi-harmonic functional comes out to be

$$Y(k, l, s, t) = \begin{pmatrix} 176/1575 & -29/1575 & -29/1575 & -83/3150 \\ -29/1575 & 176/1575 & -83/3150 & -29/1575 \\ -29/1575 & -83/3150 & 176/1575 & -29/1575 \\ -83/3150 & -29/1575 & -29/1575 & 176/1575 \end{pmatrix} \quad (77)$$

for

$$W^1(s, t) = \begin{pmatrix} -139795/252252 \\ 676703/3153150 \\ 320293/6306300 \\ -17099/126126 \end{pmatrix}, W^2(s, t) = \begin{pmatrix} 43/210 \\ -1/210 \\ -9/70 \\ 23/70 \end{pmatrix}, W^3(s, t) = \begin{pmatrix} -990751/1351350 \\ -204251/3783780 \\ -3767641/18918900 \\ -899177/4729725 \end{pmatrix}. \quad (78)$$

Simultaneous solutions of the system of equations

$$\begin{pmatrix} 176/1575 & -29/1575 & -29/1575 & -83/3150 \\ -29/1575 & 176/1575 & -83/3150 & -29/1575 \\ -29/1575 & -83/3150 & 176/1575 & -29/1575 \\ -83/3150 & -29/1575 & -29/1575 & 176/1575 \end{pmatrix} \begin{pmatrix} x_{uv}^a(0, 0) \\ x_{uv}^a(0, 1) \\ x_{uv}^a(1, 0) \\ x_{uv}^a(1, 1) \end{pmatrix} = \begin{pmatrix} W^a(0, 0) \\ W^a(0, 1) \\ W^a(1, 0) \\ W^a(1, 1) \end{pmatrix} \quad (79)$$

for the unknown MPDs  $x_{uv}(0, 0)$ ,  $x_{uv}(0, 1)$ ,  $x_{uv}(1, 0)$  and  $x_{uv}(1, 1)$  for the quasi-harmonic functional are then determined, and they are

$$\begin{aligned}
 x_{uv}(0, 0) &= \left( \frac{3222470572}{569984415}, -\frac{16129}{5423}, \frac{1784415566}{189994805} \right), \\
 x_{uv}(0, 1) &= \left( -\frac{82691645}{227993766}, -\frac{6201}{5423}, \frac{4740714149}{1139968830} \right), \\
 x_{uv}(1, 0) &= \left( \frac{469443346}{569984415}, -\frac{1339}{5423}, \frac{5939053907}{1139968830} \right), \\
 x_{uv}(1, 1) &= \left( \frac{229944563}{87689910}, -\frac{20991}{5423}, \frac{1037281563}{189994805} \right). \quad (80)
 \end{aligned}$$

For these values of MPDs  $\mathbf{x}_{uv}(0,0)$ ,  $\mathbf{x}_{uv}(0,1)$ ,  $\mathbf{x}_{uv}(1,0)$  and  $\mathbf{x}_{uv}(1,1)$ , the BBCP Equation (23) can be found which is the extremal of the quasi-harmonic functional Equation (53) for the optimal twist vectors given by Equation (80). The BBCP Equation (23), along with the twist vectors Equation (80) (shown in Figure 6), comes out to be

$$\begin{aligned}
 x(u,v) &= -\frac{241817u^3v^3}{51051} + \frac{30137598u^3v^2}{2467465} - \frac{6849562u^3v}{1057485} + \frac{39616099u^2v^3}{4934930} - \frac{7660029283u^2v^2}{379989610} + \\
 &\quad \frac{35458382u^2v}{2922997} - \frac{48721367uv^3}{14804790} + \frac{3018839191uv^2}{379989610} - \frac{3222470572uv}{569984415} + u \\
 y(u,v) &= \frac{140u^3v^3}{17} - \frac{5648u^3v^2}{493} + \frac{1588u^3v}{493} - \frac{210u^2v^3}{17} + \frac{100587u^2v^2}{5423} - \frac{33597u^2v}{5423} + \frac{70uv^3}{17} - \\
 &\quad \frac{38459uv^2}{5423} + \frac{16129uv}{5423} + v^2 \\
 z(u,v) &= -\frac{1134349u^3v^3}{51051} + \frac{201452103u^3v^2}{4934930} - \frac{39342157u^3v}{2114970} + \frac{30370023u^2v^3}{986986} - \frac{33494646292u^2v^2}{569984415} + \\
 &\quad \frac{34191853679u^2v}{1139968830} - u^2 - \frac{28278785uv^3}{2960958} + \frac{21593825621uv^2}{1139968830} - \frac{2164405176uv}{189994805} + u - v^2 + v
 \end{aligned} \tag{81}$$

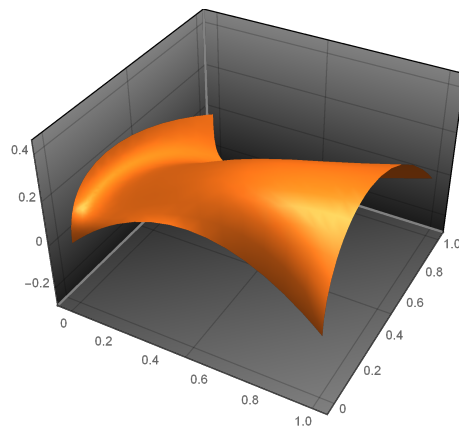


**Figure 6.** The bicubically blended Coons patch Equation (81) as the extremal solution of quasi-harmonic functional Equation (53).

In a similar fashion, we can find the MPDs as the solution of the simultaneous system of equations (50) as the extremal of the Dirichlet functional (38) for which the BBCP Equation (23) is the extremal of the Dirichlet functional (38). After obtaining the optimal BBCP using the optimal twist vectors, such as the one given by the above Equation (81), the fundamental coefficients  $E$ ,  $F$ ,  $G$  and the numerator of mean curvature  $H$  (see Appendix A, Equations (A1)–(A8)) of the BBCP (see Equation (70)) have already been determined, and in this case, the line element can be written as  $ds^2 = Edu^2 + 2Fdudv + Gdv^2$ . In the context of minimal surfaces, the mean curvature of the surface should be identically equal to zero, resulting in a non-linear second-order partial differential equation known as the minimal surface equation. The investigation of the Lie group of symmetries associated with minimal surfaces can be carried out by employing the symmetry groups of differential equations [7,8]. Notably, Bila [9] (p. 4) has suggested that for a surface in Monge's form, the Lie group of symmetries can be generated from seven vector fields. Therefore, an interesting research avenue would be to explore the Lie symmetries of the minimal surface equation resulting from the optimal BBCP. This exploration of Lie symmetries in the context of related partial differential equations for the minimal surface equation holds the potential to present a challenging yet captivating research problem for future investigation.

## 6. Conclusions

The construction of the Coons patch taken into account is based on the Hermite cubic interpolants, called a bicubically blended Coons patch (BBCP), which is composed of (a) four corner points, (b) eight tangent vectors, and (c) four twist vectors. The interior shape of the BBCP depends not only on the tangent vectors at the corner points but also on the twist vectors. However, by keeping the same arrangement of the tangent vectors at the corner points, the interior shape can still be changed by alteration in the twist vectors at these corner points. A method for finding the twist vectors (MPDs) of the patch by extremizing the Dirichlet functional and quasi-harmonic functional is presented, and this method can be used to generate a quasi-minimal BBCP (as the extremal of the Dirichlet functional) and a quasi-harmonic BBCP as the extremal of a quasi-harmonic functional taken over the whole surface. For the twist vectors obtained by the approach followed, we can find a quasi-minimal BBCP (BBCP) and a quasi-harmonic BBCP. One potential application of this work is in the fuzzy optimal control problems, where fuzzy constraints are used to model uncertainty and imprecision in the system being controlled. The presented method for generating quasi-minimal BBCPs and quasi-harmonic BBCPs can be applied to fuzzy optimal control problems to obtain more accurate and robust solutions. This application could lead to improved control of complex systems, such as those found in aerospace engineering or robotics. We can find the appropriate such twist vectors by varying the corner points and the corresponding tangent vectors, as for example, the MPDs as the extremal of a quasi-harmonic function are determined and given in Equation (80), for which the BBCP Equation (81) appears as the extremal of the quasi-harmonic functional (53). This study has made contributions to the understanding and optimization of BBCPs. Future research endeavors could focus on symmetry consideration and investigating the symmetries exhibited by these patches and exploring their geometric properties. These avenues hold great potential for advancing the field of surface optimization and related areas.

**Author Contributions:** D.A. conceived and supervised the project. K.N. developed the theoretical framework and wrote the manuscript with input from Daud Ahmad. M.E.B. provided support in performing calculations and generating examples. P.C.D. and M.S. provided technical input and feedback throughout the project. All authors reviewed and edited the manuscript. All authors have read and agreed to the published version of the manuscript.

**Funding:** This research was partially supported by the project 38 PFE in the frame of the program PDI-PFE-CDI 2021.

**Data Availability Statement:** Not available.

**Conflicts of Interest:** The authors declare that they have no conflicts of interest.

## Appendix A. Fundamental Magnitudes, Mean Curvature, and Gaussian Curvature of BBCP

The fundamental coefficients of the metric element of the BBCP are

$$E(u, v) = 180u^4v^6 - 144u^4v^5 - 27u^4v^4 - 144u^4v^3 + 144u^4v^2 - 456u^3v^6 + 408u^3v^5 + 336u^3v^4 - 24u^3v^3 - 312u^3v^2 + 48u^3v + 436u^2v^6 - 564u^2v^5 - 270u^2v^4 + 308u^2v^3 + 162u^2v^2 - 72u^2v + 4u^2 - 160u \times v^6 + 280uv^5 + 32uv^4 - 188uv^3 + 4uv^2 + 32uv - 4u + 20v^6 - 44v^5 + 9v^4 + 28v^3 - 10v^2 - 4v + 2, \quad (A1)$$

$$F(u, v) = 180u^5v^5 - 120u^5v^4 - 18u^5v^3 - 72u^5v^2 + 48u^5v - 570u^4v^5 + 412u^4v^4 + 296u^4v^3 - 24u^4v^2 - 128 \times u^4v + 8u^4 + 702u^3v^5 - 728u^3v^4 - 332u^3v^3 + 260u^3v^2 + 90u^3v - 16u^3 - 360u^2v^5 + 502u^2v^4 + 52 \times u^2v^3 - 177u^2v^2 - 14u^2v + 10u^2 + 60uv^5 - 82uv^4 - 8uv^3 + 24uv^2 + 6uv - 4u - 8v^4 + 12v^3 - 4v + 1, \quad (A2)$$

$$G(u, v) = 180u^6v^4 - 96u^6v^3 + 4u^6v^2 - 32u^6v + 16u^6 - 684u^5v^4 + 408u^5v^3 + 144u^5v^2 - 48u^5 + 1053u^4v^4 - 900u^4v^3 - 184u^4v^2 + 120u^4v + 52u^4 - 720u^3v^4 + 816u^3v^3 - 16u^3v^2 - 96u^3v - 32u^3 + 180u^2v^4 - 180u^2v^3 - 14u^2v^2 + 20u^2v + 16u^2 - 48uv^3 + 56uv^2 - 8uv - 4u + 8v^2 - 4v + 1, \quad (A3)$$

$$e(u, v) = -252u^5v^4 + 384u^5v^3 - 72u^5v^2 - 96u^4v^5 + 594u^4v^4 - 960u^4v^3 + 252u^4v^2 + 144u^3v^5 - 516u^3v^4 + 832u^3 \times v^3 - 288u^3v^2 + 8u^3 - 60u^2v^5 + 198u^2v^4 - 312u^2v^3 + 120u^2v^2 - 12u^2 - 24uv^4 + 56uv^3 - 24uv^2 + 4u - 4v^3 + 6v^2 - 2, \quad (A4)$$

$$f(u, v) = -252u^4v^5 + 576u^4v^4 - 216u^4v^3 + 396u^3v^5 - 1152u^3v^4 + 648u^3v^3 - 72u^3v^2 - 228u^2v^5 + 768u^2v^4 - 576u^2v^3 + 156u^2v^2 - 24u^2v + 60uv^5 - 192uv^4 + 132uv^3 - 48uv^2 + 24uv - 8v^5 + 16v^4 - 4v^2 - 4v, \quad (A5)$$

$$g(u, v) = 192u^2v^7 - 396u^2v^6 + 252u^2v^5 - 24u^2v^4 - 36u^2v^3 - 144uv^7 + 312uv^6 - 216uv^5 + 48uv^4 + 60uv^3 - 48uv^2 + 40v^7 - 84v^6 + 60v^5 - 36v^4 + 24v^2 - 4v, \quad (A6)$$

and  $w = EG - F^2$  is

$$w = 1764v^8u^{10} - 8064v^7u^{10} + 12240v^6u^{10} - 6912v^5u^{10} + 1296v^4u^{10} + 4032v^9u^9 - 23076v^8u^9 + 58824 \times v^7u^9 - 77616v^6u^9 + 47808v^5u^9 - 12240v^4u^9 + 864v^3u^9 + 2304v^{10}u^8 - 21888v^9u^8 + 84081v^8u^8 - 171492v^7u^8 + 207768v^6u^8 - 137064v^5u^8 + 44772v^4u^8 - 6528v^3u^8 + 432v^2u^8 - 6912v^{10}u^7 + 44520 \times v^9u^7 - 140232v^8u^7 + 253560v^7u^7 - 292824v^6u^7 + 205260v^5u^7 - 81432v^4u^7 + 18120v^3u^7 - 2352 \times v^2u^7 + 96vu^7 + 8064v^{10}u^6 - 42156v^9u^6 + 115402v^8u^6 - 190388v^7u^6 + 214264v^6u^6 - 161156v^5u^6 + 76468v^4u^6 - 23552v^3u^6 + 4732v^2u^6 - 416vu^6 + 16u^6 - 4320v^{10}u^5 + 16824v^9u^5 - 36924v^8u^5 + 50664 \times v^7u^5 - 55068v^6u^5 + 49416v^5u^5 - 31608v^4u^5 + 14280v^3u^5 - 4248v^2u^5 + 600vu^5 - 48u^5 + 900v^{10}u^4 + 204v^9u^4 - 6079v^8u^4 + 17592v^7u^4 - 21998v^6u^4 + 10652v^5u^4 + 678v^4u^4 - 3260v^3u^4 + 1736v^2u^4 - 360vu^4 + 52u^4 - 1776v^9u^3 + 4568v^8u^3 - 10536v^7u^3 + 15556v^6u^3 - 9388v^5u^3 + 1464v^4u^3 + 460v^3 \times u^3 - 448v^2u^3 + 132vu^3 - 32u^3 + 240v^9u^2 + 1256v^8u^2 - 1804v^7u^2 - 1586v^6u^2 + 1656v^5u^2 + 554v^4 \times u^2 - 380v^3u^2 + 116v^2u^2 - 52vu^2 + 16u^2 - 800v^8u + 1664v^7u - 536v^6u - 456v^5u + 80v^4u + 4v^3u + 28v^2u + 4vu - 4u + 96v^8 - 240v^7 + 124v^6 + 80v^5 - 71v^4 + 12v^3 + 6v^2 - 4v + 1. \quad (A7)$$

The numerator of the mean curvature of the BBCP is as follows:

$$\begin{aligned}
H_n = & 34560u^6v^{13} - 113472u^5v^{13} + 156576u^4v^{13} - 111744u^3v^{13} + 44320u^2v^{13} - 9280uv^{13} + 800v^{13} - \\
& 98928u^6v^{12} + 335808u^5v^{12} - 502848u^4v^{12} + 388992u^3v^{12} - 165792u^2v^{12} + 37216uv^{12} - 3440v^{12} + \\
& 97200u^6v^{11} - 291888u^5v^{11} + 480600u^4v^{11} - 424512u^3v^{11} + 204240u^2v^{11} - 51184uv^{11} + 5256v^{11} + \\
& 90720u^9v^{10} - 429840u^8v^{10} + 887328u^7v^{10} - 1076508u^6v^{10} + 734904u^5v^{10} - 311916u^4v^{10} + 133296 \times \\
& u^3v^{10} - 68356u^2v^{10} + 22552uv^{10} - 2996v^{10} - 17280u^{10}v^9 - 176256u^9v^9 + 1163664u^8v^9 - 2884608 \times \\
& u^7v^9 + 3899328u^6v^9 - 2969640u^5v^9 + 1169428u^4v^9 - 148304u^3v^9 - 39212u^2v^9 + 12840uv^9 - 756v^9 \\
& - 45360u^{11}v^8 + 288504u^{10}v^8 - 610596u^9v^8 + 279234u^8v^8 + 1423044u^7v^8 - 3473058u^6v^8 + 3581016 \times \\
& u^5v^8 - 1809444u^4v^8 + 338240u^3v^8 + 53216u^2v^8 - 29104uv^8 + 2964v^8 + 93312u^{11}v^7 - 595680u^{10}v^7 + \\
& 1648800u^9v^7 - 2822328u^8v^7 + 2988240u^7v^7 - 1413444u^6v^7 - 396468u^5v^7 + 717572u^4v^7 - 203568u^3 \times \\
& v^7 - 36452u^2v^7 + 23980uv^7 - 2712v^7 - 50832u^{11}v^6 + 312600u^{10}v^6 - 892584u^9v^6 + 1787316u^8v^6 - \\
& 2692104u^7v^6 + 2645892u^6v^6 - 1410168u^5v^6 + 273666u^4v^6 + 43024u^3v^6 - 17544u^2v^6 - 288uv^6 + 216 \times \\
& v^6 + 16512u^{11}v^5 - 22656u^{10}v^5 - 103520u^9v^5 + 293184u^8v^5 - 152288u^7v^5 - 313976u^6v^5 + 470768u^5 \times \\
& v^5 - 204284u^4v^5 - 6328u^3v^5 + 31164u^2v^5 - 9664uv^5 + 1044v^5 - 16608u^{11}v^4 + 42960u^{10}v^4 + 40144 \times \\
& u^9v^4 - 306120u^8v^4 + 537704u^7v^4 - 441340u^6v^4 + 142664u^5v^4 + 15136u^4v^4 - 13900u^3v^4 - 2990u^2 \times \\
& v^4 + 2376uv^4 - 296v^4 + 8448u^{11}v^3 - 41856u^{10}v^3 + 79168u^9v^3 - 59040u^8v^3 - 30048u^7v^3 + 98208u^6 \times \\
& v^3 - 71088u^5v^3 + 12296u^4v^3 + 6816u^3v^3 - 3472u^2v^3 + 872uv^3 - 116v^3 - 1152u^{11}v^2 + 7488u^{10}v^2 - \times \\
& 20416u^9v^2 + 32256u^8v^2 - 30064u^7v^2 + 10424u^6v^2 + 6040u^5v^2 - 5860u^4v^2 + 1544u^3v^2 - 164u^2v^2 - \times \\
& 144uv^2 + 30v^2 - 256u^9v + 384u^8v + 832u^7v - 1760u^6v + 640u^5v + 384u^4v - 464u^3v + 280u^2v - 64u \times \\
& v + 8v + 128u^9 - 576u^8 + 1056u^7 - 1104u^6 + 816u^5 - 456u^4 + 184u^3 - 60u^2 + 12u - 2,
\end{aligned} \tag{A8}$$

The numerator of the Gaussian curvature of the BBCP, denoted by  $G_n = s = eg - f^2$ , is given by

$$\begin{aligned}
G_n = & -63504u^8v^{10} + 290304u^8v^9 - 440640u^8v^8 + 248832u^8v^7 - 46656u^8v^6 - 48384u^7v^{11} + 373104 \times \\
& u^7v^{10} - 1266192u^7v^9 + 1956096u^7v^8 - 1298736u^7v^7 + 350784u^7v^6 - 28512u^7v^5 - 18432u^6v^{12} + \\
& 188352u^6v^{11} - 849384u^6v^{10} + 2327256u^6v^9 - 3583872u^6v^8 + 2707992u^6v^7 - 966240u^6v^6 + \\
& 156528u^6v^5 - 12096u^6v^4 + 41472u^5v^{12} - 281664u^5v^{11} + 992016u^5v^{10} - 2336688u^5v^9 + 3512592 \times \\
& u^5v^8 - 2888856u^5v^7 + 1256256u^5v^6 - 304992u^5v^5 + 48384u^5v^4 - 3456u^5v^3 - 36096u^4v^{12} + \\
& 212832u^4v^{11} - 662928u^4v^{10} + 1404960u^4v^9 - 2013624u^4v^8 + 1699176u^4v^7 - 826032u^4v^6 + \\
& 264264u^4v^5 - 67344u^4v^4 + 10848u^4v^3 - 960u^4v^2 + 14400u^3v^{12} - 84576u^3v^{11} + 258880u^3v^{10} - \\
& 521472u^3v^9 + 699072u^3v^8 - 556888u^3v^7 + 263280u^3v^6 - 97440u^3v^5 + 36608u^3v^4 - 10080u^3 \times \\
& v^3 + 1920u^3v^2 - 32u^3v - 2400u^2v^{12} + 16416u^2v^{11} - 56280u^2v^{10} + 116520u^2v^9 - 146544u^2v^8 + \\
& 99144u^2v^7 - 32712u^2v^6 + 9480u^2v^5 - 6048u^2v^4 + 3192u^2v^3 - 1248u^2v^2 + 48u^2v - 960uv^{11} + \\
& 5792uv^{10} - 14208uv^9 + 17232uv^8 - 9008uv^7 + 240uv^6 + 1416uv^5 - 656uv^4 - 216uv^3 + 384u \times \\
& v^2 - 16uv - 224v^{10} + 832v^9 - 1000v^8 + 360v^7 + 16v^6 - 88v^5 + 216v^4 - 56v^3 - 64v^2 + 8v
\end{aligned} \tag{A9}$$

## References

1. Barrera, D.; Fortes, M.A.; González, P.; Pasadas, M. Minimal energy-surfaces on uniform Powell–Sabin–type meshes for noisy data. *J. Comput. Appl. Math.* **2008**, *2*, 592–602. [\[CrossRef\]](#)
2. Jiao, X.; Wang, D.; Zha, H. Simple and effective variational optimization of surface and volume triangulations. *Eng. Comput.* **2011**, *27*, 81–94. [\[CrossRef\]](#)
3. Stephani, H.; Kramer, D.; MacCallum, M.; Hoenselaers, C.; Herlt, E. *Exact Solutions of Einstein's Field Equations*, 2nd ed.; Cambridge Monographs on Mathematical Physics; Cambridge University Press: Cambridge, UK, 2003. [\[CrossRef\]](#)

4. Misner, C.W.; Thorne, K.S.; Wheeler, J.A. *Gravitation*; W. H. Freeman: San Francisco, CA, USA 1973.
5. Jayadevan, V.; Sawada, T.; Delp, E.; Pizlo, Z. Perception of 3D Symmetrical and Nearly Symmetrical Shapes. *Symmetry* **2018**, *10*, 344. [\[CrossRef\]](#)
6. Grundland, A.; Hariton, A. Algebraic Aspects of the Supersymmetric Minimal Surface Equation. *Symmetry* **2017**, *9*, 318. [\[CrossRef\]](#)
7. Bluman, G.W.; Kumei, S. *Symmetries and Differential Equations*, 1st ed.; Applied Mathematical Sciences; Springer: New York, NY, USA, 1989; p. XIII, 413. [\[CrossRef\]](#)
8. Olver, P.J. *Applications of Lie Groups to Differential Equations*, 2nd ed.; Graduate Texts in Mathematics; Springer: New York, NY, USA, 1993; p. XXVIII, 513. [\[CrossRef\]](#)
9. Bila, N. Lie groups applications to minimal surfaces PDE. *Differ. Geom.-Dyn. Syst.* **1999**, *1*, 1–9.
10. Oliveri, F. Lie Symmetries of Differential Equations: Classical Results and Recent Contributions. *Symmetry* **2010**, *2*, 658–706. [\[CrossRef\]](#)
11. Ibragimov, N.H. *Lie Group Analysis: Classical Heritage*; ALGA Publications: Deakin, Australia, 2004; p. 157.
12. Ahmad, D.; Ziad, M. Homothetic motions of spherically symmetric space-times. *J. Math. Phys.* **1997**, *38*, 2547–2552. [\[CrossRef\]](#)
13. Ahmad, D.; Habib, K. Homotheties of a Class of Spherically Symmetric Space-Time Admitting  $G_3$  as Maximal Isometry Group. *Adv. Math. Phys.* **2018**, *2018*, 8195208. [\[CrossRef\]](#)
14. Osserman, R. *A Survey of Minimal Surfaces*; Dover Publications Inc.: New York, USA, 1986.
15. Nitsche, J.C.C. *Lectures on Minimal Surfaces*; Cambridge University Press: Cambridge, UK, 1989.
16. Coppin, C.; Greenspan, D. A contribution to the particle modeling of soap films. *Appl. Math. Comput.* **1988**, *26*, 315–331. [\[CrossRef\]](#)
17. Douglas, J. Solution of the problem of Plateau. *Trans. Am. Math. Soc.* **1931**, *33*, 263–321. [\[CrossRef\]](#)
18. Osserman, R. A Proof of the Regularity Everywhere of the Classical Solution to Plateau’s Problem. *Ann. Math.* **1970**, *91*, 550–569. [\[CrossRef\]](#)
19. Ahmad, D.; Masud, B. A Coons Patch Spanning a Finite Number of Curves Tested for Variationally Minimizing Its Area. *Abstr. Appl. Anal.* **2013**, *2013*, 645368. [\[CrossRef\]](#)
20. Ahmad, D.; Masud, B. Variational minimization on string-rearrangement surfaces, illustrated by an analysis of the bilinear interpolation. *Appl. Math. Comput.* **2014**, *233*, 72–84. [\[CrossRef\]](#)
21. Ahmad, D.; Masud, B. Near-stability of a quasi-minimal surface indicated through a tested curvature algorithm. *Comput. Math. Appl.* **2015**, *69*, 1242–1262. [\[CrossRef\]](#)
22. Ahmad, D.; Naem, S. Quasi-Harmonic Constraints For Toric Bézier Surfaces. *Sigma J. Eng. Nat. Sci.* **2018**, *36*, 325–340.
23. Ahmad, D.; Hassan, K.; Mahmood, M.K.; Ali, J.; Khan, I.; Fayz-Al-Asad, M. Variationally Improved Bézier Surfaces with Shifted Knots. *Adv. Math. Phys.* **2021**, *2021*, 9978633. [\[CrossRef\]](#)
24. Nisar, K.S.; Ali, J.; Mahmood, M.K.; Ahmad, D.; Ali, S. Hybrid evolutionary padé approximation approach for numerical treatment of nonlinear partial differential equations. *Alex. Eng. J.* **2021**, *60*, 4411–4421. [\[CrossRef\]](#)
25. Ahmad, D.; Mahmood, M.K.; Xin, Q.; Tawfiq, F.M.O.; Bashir, S.; Khalid, A. A Computational Model for  $q$ -Bernstein Quasi-Minimal Bézier Surface. *J. Math.* **2022**, *2022*, 8994112. [\[CrossRef\]](#)
26. Farin, G.E.; Hansford, D. Discrete Coons patches. *Comput. Aided Geom. Des.* **1999**, *16*, 691–700. [\[CrossRef\]](#)
27. Szilvási-Nagy, M.; Szabó, I.  $C^1$ -continuous Coons-type blending of triangular patches. *KoG* **2005**, *9*, 29–34.
28. Wang, C.C.L.; Tang, K. Non-self-overlapping Hermite interpolation mapping: A practical solution for structured quadrilateral meshing. *Comput.-Aided Des.* **2005**, *37*, 271–283. [\[CrossRef\]](#)
29. Farouki, R.; Szafran, N.; Biard, L. Existence conditions for Coons patches interpolating geodesic boundary curves. *Comput.-Aided Geom. Des.* **2009**, *26*, 599–614. [\[CrossRef\]](#)
30. Liu, F.; Ji, X.; Hu, G.; Gao, J. A Novel Shape-Adjustable Surface and Its Applications in Car Design. *Appl. Sci.* **2019**, *9*, 2339. [\[CrossRef\]](#)
31. Monterde, J. Bézier surfaces of minimal area: The Dirichlet approach. *Comput.-Aided Geom. Des.* **2004**, *21*, 117–136. [\[CrossRef\]](#)
32. Monterde, J.; Ugail, H. On harmonic and biharmonic Bézier surfaces. *Comput.-Aided Geom. Des.* **2004**, *21*, 697–715. [\[CrossRef\]](#)
33. Chen, X.D.; Xu, G.; Wang, Y. Approximation methods for the Plateau-Bézier problem. In Proceedings of the 2009 11th IEEE International Conference on Computer-Aided Design and Computer Graphics, Huangshan, China, 19–21 August 2009.
34. Xu, G.; Rabczuk, T.; Güler, E.; Wu, Q.; Hui, K.C.; Wang, G. Quasi-harmonic Bézier Approximation of Minimal Surfaces for Finding Forms of Structural Membranes. *Comput. Struct.* **2015**, *161*, 55–63. [\[CrossRef\]](#)
35. Velimirović, L.S.; Ćirić, M.S.; Cvetković, M.D. Change of the Willmore energy under infinitesimal bending of membranes. *Comput. Math. Appl.* **2010**, *59*, 3679–3686. [\[CrossRef\]](#)
36. Li, X.; Zhu, Y.; Wu, H.; Xu, J.; Ling, R.; Wu, X.; Xu, G. Construction of Bézier surfaces with energy-minimizing diagonal curves from given boundary. *J. Comput. Appl. Math.* **2022**, *413*, 114382. [\[CrossRef\]](#)
37. Bates, P.W.; Wei, G.W.; Zhao, S. Minimal molecular surfaces and their applications. *J. Comput. Chem.* **2008**, *29*, 380–391. [\[CrossRef\]](#)
38. Zhu, C.; Gu, P.; Liu, D.; Hu, X.; Wu, Y. Evaluation of surface topography of SiCp/Al composite in grinding. *Int. J. Adv. Manuf. Technol.* **2019**, *102*, 2807–2821. [\[CrossRef\]](#)
39. Liu, Y.; Yang, S.; Li, D.; Zhang, S. Improved Whale Optimization Algorithm for Solving Microgrid Operations Planning Problems. *Symmetry* **2022**, *15*, 36. [\[CrossRef\]](#)

40. Wang, D.; Zhang, J.; Zhang, T.; Zhang, H.; Peng, Y. A Coupling Optimization Method of Vehicle Structure and Restraint System for Occupant Injury Protection in Traffic Accidents. *Symmetry* **2023**, *15*, 558. [[CrossRef](#)]
41. Zhao, Y.; Liu, Y.; Wu, Z.; Zhang, S.; Zhang, L. Improving Sparrow Search Algorithm for Optimal Operation Planning of Hydrogen–Electric Hybrid Microgrids Considering Demand Response. *Symmetry* **2023**, *15*, 919. [[CrossRef](#)]
42. Herty, M.; Klar, A. Modeling, Simulation, and Optimization of Traffic Flow Networks. *SIAM J. Sci. Comput.* **2003**, *25*, 1066–1087. [[CrossRef](#)]
43. D’Apice, C.; Göttlich, S.; Herty, M.; Piccoli, B. *Modeling, Simulation, and Optimization of Supply Chains*; Society for Industrial and Applied Mathematics: Philadelphia, PA, USA, 2010. [[CrossRef](#)]
44. Pinnau, R.; Siedow, N. Optimization and Inverse Problems in Radiative Heat Transfer. In *Constrained Optimization and Optimal Control for Partial Differential Equations*; Leugering, G., Engell, S., Griewank, A., Hinze, M., Rannacher, R., Schulz, V., Ulbrich, M., Ulbrich, S., Eds.; Springer: Basel, Switzerland, 2012; pp. 597–609. [[CrossRef](#)]
45. Repke, S.; Marheineke, N.; Pinnau, R. *On Adjoint-Based Optimization of a Free Surface Stokes Flow*; Technical Report 186; Fraunhofer (ITWM): Kaiserslautern, Germany, 2010.
46. Marheineke, N.; Pinnau, R. Model Hierarchies in Space-Mapping Optimization: Feasibility Study for Transport Processes. *J. Comp. Methods Sci. Eng.* **2012**, *12*, 63–74. [[CrossRef](#)]
47. Drago, C.; Marheineke, N.; Pinnau, R. Semiconductor device optimization in the presence of thermal effects. *ZAMM—J. Appl. Math. Mech.* **2013**, *93*, 700–705. [[CrossRef](#)]
48. Ahmad, D.; Naz, K.; Bashir, S.; Bariq, A. An Application of Variational Minimization: Quasi-Harmonic Coon’s Patches. *J. Funct. Spaces* **2022**, *2022*, 8067097. [[CrossRef](#)]
49. Farin, G. *Curves and Surfaces for CAGD*; The Morgan Kaufmann Series in Computer Graphics; Morgan Kaufmann: San Francisco, CA, USA, 2002. [[CrossRef](#)]
50. Yamaguchi, F. *Curves and Surfaces in Computer Aided Geometric Design*; Springer: Berlin/Heidelberg, Germany, 2012.
51. Filev, D.; Angelov, P. Fuzzy optimal control. *Fuzzy Sets Syst.* **1992**, *47*, 151–156. [[CrossRef](#)]
52. Farhadinia, B. Necessary optimality conditions for fuzzy variational problems. *Inf. Sci.* **2011**, *181*, 1348–1357. [[CrossRef](#)]
53. Mustafa, A.M.; Gong, Z.; Osman, M. The solution of fuzzy variational problem and fuzzy optimal control problem under granular differentiability concept. *Int. J. Comput. Math.* **2021**, *98*, 1495–1520. [[CrossRef](#)]
54. Puri, L.M.; Ralescu, D.A. Differentials of fuzzy functions. *J. Math. Anal. Appl.* **1982**, *91*, 552–558. [[CrossRef](#)]
55. Sahinidis, N. Optimization under uncertainty: State-of-the-art and opportunities. *Comput. Chem. Eng.* **2004**, *28*, 971–983. [[CrossRef](#)]
56. Agrawal, O.P.; Baleanu, D. A Hamiltonian Formulation and a Direct Numerical Scheme for Fractional Optimal Control Problems. *J. Vib. Control* **2007**, *13*, 1269–1281. [[CrossRef](#)]
57. Agrawal, O.P. Generalized Euler-Lagrange equations and transversality conditions for FVPs in terms of the Caputo derivative. *J. Vib. Control* **2007**, *13*, 1217–1237. [[CrossRef](#)]
58. Untiedt, E.A.; Lodwick, W.A. On selecting an algorithm for fuzzy optimization. In *Proceedings of the Foundations of Fuzzy Logic and Soft Computing: 12th International Fuzzy System Association World Congress, IFSA 2007, Cancun, Mexico, 18–21 June 2007*; Springer: Berlin/Heidelberg, Germany, 2007; pp. 371–380.
59. Nguyen, T.V.T.; Huynh, N.T.; Vu, N.C.; Kieu, V.N.D.; Huang, S.C. Optimizing compliant gripper mechanism design by employing an effective bi-algorithm: Fuzzy logic and ANFIS. *Microsyst. Technol.* **2021**, *27*, 3389–3412. [[CrossRef](#)]
60. Huynh, N.T.; Nguyen, T.V.T.; Tam, N.T.; Nguyen, Q.M. Optimizing Magnification Ratio for the Flexible Hinge Displacement Amplifier Mechanism Design. In *Proceedings of the 2nd Annual International Conference on Material, Machines and Methods for Sustainable Development (MMMS2020), Nha Trang, Vietnam, 12–15 November 2020*; pp. 769–778.
61. Batool, S.; Hashmi, M.R.; Riaz, M.; Smarandache, F.; Pamucar, D.; Spasic, D. An Optimization Approach with Single-Valued Neutrosophic Hesitant Fuzzy Dombi Aggregation Operators. *Symmetry* **2022**, *14*, 2271. [[CrossRef](#)]
62. Akram, M.; Shah, S.M.U.; Al-Shamiri, M.A.; Edalatpanah, S.A. Extended DEA method for solving multi-objective transportation problem with Fermatean fuzzy sets. *AIMS Math.* **2022**, *8*, 924–961. [[CrossRef](#)]
63. Akram, M.; Shah, S.M.U.; Al-Shamiri, M.A.; Edalatpanah, S.A. Fractional transportation problem under interval-valued Fermatean fuzzy sets. *AIMS Math.* **2022**, *7*, 17327–17348. [[CrossRef](#)]
64. Akram, M.; Shahzadi, S.; Shah, S.M.U.; Allahviranloo, T. An extended multi-objective transportation model based on Fermatean fuzzy sets. *Soft Comput.* **2023**. [[CrossRef](#)]

**Disclaimer/Publisher’s Note:** The statements, opinions and data contained in all publications are solely those of the individual author(s) and contributor(s) and not of MDPI and/or the editor(s). MDPI and/or the editor(s) disclaim responsibility for any injury to people or property resulting from any ideas, methods, instructions or products referred to in the content.